Environmental Science & Technology

ARTICLE

pubs.acs.org/est

Modeling the Multiday Evolution and Aging of Secondary Organic Aerosol During MILAGRO 2006

Katja Dzepina,[†,‡,∥,▽] Christopher D. Cappa,[⊥] Rainer M. Volkamer,[†,‡] Sasha Madronich,[∥] Peter F. DeCarlo,[†,§,¶] Rahul A. Zaveri,[#] and Jose L. Jimenez[†,‡,*]

[†]Cooperative Institute for Research in Environmental Sciences, [‡]Department of Chemistry and Biochemistry, and [§]Department of Atmospheric and Oceanic Sciences, University of Colorado, Boulder, Colorado

[∥]Atmospheric Chemistry Division, National Center for Atmospheric Research, Boulder, Colorado

[⊥]Department of Civil and Environmental Engineering, University of California—Davis, Davis, California

[#]Pacific Northwest National Laboratory, Richland, Washington

S *Supporting Information*

ABSTRACT: In this study, we apply several recently proposed models to the evolution of secondary organic aerosols (SOA) and organic gases advected from downtown Mexico City at an altitude of ~3.5 km during three days of aging, in a way that is directly comparable to simulations in regional and global models. We constrain the model with and compare its results to available observations. The model SOA formed from oxidation of volatile organic compounds (V-SOA) when using a non-aging SOA parameterization cannot explain the observed SOA concentrations in aged pollution, despite the increasing importance of the low-NO_x channel. However, when using an aging SOA parameterization, V-SOA alone is similar to the regional aircraft observations, highlighting the wide diversity in current V-SOA formulations. When the SOA formed from oxidation of semivolatile and intermediate volatility organic vapors (SI-SOA) is computed following Robinson et al. (2007) the model matches the observed SOA mass, but its O/C is ~2× too low. With the parameterization of Grieshop et al. (2009), the total SOA mass is ~2× too high, but O/C and volatility are closer to the observations. Heating or dilution cause the evaporation of a substantial fraction of the model SOA; this fraction is reduced by aging although differently for heating vs dilution. Lifting of the airmass to the free-troposphere during dry convection substantially increases SOA by condensation of semivolatile vapors; this effect is reduced by aging.

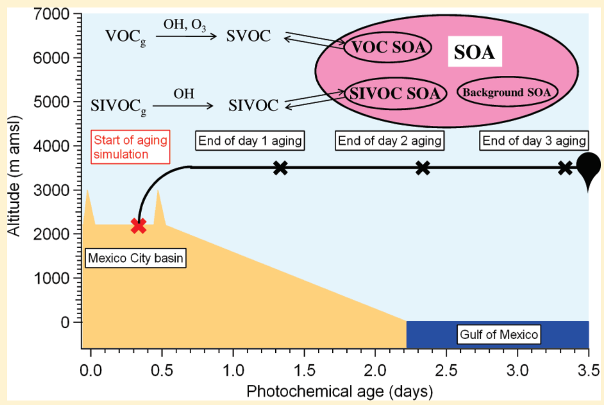

1. INTRODUCTION

Atmospheric aerosols impact the global radiation balance, climate change, and air quality. Approximately one-half of the total fine particulate mass in the atmosphere is comprised of organic aerosols (OA).[1] OA can be divided into primary emitted ("POA") and secondary ("SOA") species, which are formed from chemical reactions. Given the complex chemical composition, multitude of sources, and complex processing,[2] OA is one of the least understood components of ambient aerosols. Thus, characterization of the sources, composition, and concentration of ambient OA, along with OA formation and transformation processes, is important.

SOA modeling is based on absorptive partitioning theory [3] where semivolatile products formed from chemical reactions absorb into pre-existing OA, forming SOA. The gas/particle equilibrium depends on physical properties of the aerosol constituents, the amount of OA and temperature. Traditionally only volatile organic compounds (VOC) were considered in SOA modeling ("V−SOA", following the terminology of ref 4). Older models used one and two lumped semivolatile products with empirically derived amounts and partitioning parameters.[5] More recently V-SOA has been re-parameterized using a volatility basis-set framework,[6] which allows more continuous variation of SOA formation vs OA concentration and more realistic enthalpies of vaporization (ΔH_{vap}). Most V-SOA models do not reproduce SOA concentrations observed in polluted areas (refs 7 and 8 and references therein), although they appear to perform well in clean biogenic-dominated regions (e.g., 9). Some recent parametrizations invoking gas-phase aging of semivolatile products result in V-SOA loadings sufficient to match the ambient observations in polluted areas.[4] Recently, it was recognized that

Received: September 18, 2010
Accepted: February 27, 2011
Revised: January 27, 2011
Published: March 22, 2011

combustion POA is semivolatile,[10] and that the atmospheric evolution of POA is much more dynamic than previously thought. Semivolatile POA constituents quickly evaporate in the ambient atmosphere following post-emission dilution, and together with gas-phase intermediate volatility species (with volatility lower than traditional SOA precursors) form a previously unrecognized SOA precursor pool.[10] We refer to these species as primary SIVOC (P-$SIVOC_{g+p}$, where the subscripts g and p refer to the gas and particle phases, respectively) and to the SOA formed from them as SI-SOA.[4] Finally, new findings show that low molecular weight (MW) species, such as glyoxal, can form SOA via oligomerization in the aerosol aqueous phase (G-SOA),[11,12] while previously such precursors and processes were not considered to form SOA.[13]

The MILAGRO field campaign in March 2006 examined the formation and evolution of trace gases and particulate matter emitted in Mexico City over local, regional and large-scale domains.[14] Model-measurement comparisons in Mexico City show that concentrations of SOA are several-fold larger than predicted with V-SOA models (e.g., refs 7,8,15,16). The aging V-SOA model is an exception, as when compared to non-aging V-SOA one, it results in much higher model V-SOA loadings.[4] The combination of newly proposed SI-SOA, G-SOA, and updated non-aging V-SOA models can close the measured vs modeled SOA gap in Mexico City,[8,17] although some disagreements remain, and the model combination is underconstrained by the available data.

Here, we present a study in which the formation and evolution of SOA formed within Mexico City [8] continues over 3 days under realistic aging conditions, with results that are directly relevant to SOA simulations in regional and global models. The model results are compared against available MILAGRO measurements. Model SOA is characterized in the terms of its concentration, O/C ratio, volatility, and evolution during rapid lifting to free troposphere.

2. SOA MODELING METHODS

Applied modeling methods are described in detail elsewhere (ref 8 and references therein) and only an overview and modeling differences from ref 8 are given here. The model used here accounts for SOA formed from gas-phase oxidation of two sets of precursors: (1) traditional VOC (V-SOA); and (2) primary and secondary $SIVOC_g$ (SI-SOA) (Figure S1, with "S" standing here for Supporting Information). We also include in the total model SOA a small amount of background SOA (BG-SOA), with a concentration derived from observations (1.4 $\mu g\ m^{-3}$). On the basis of the observation that very aged SOA has low volatility,[18] BG-SOA is considered non-volatile, and its concentration is reduced by dilution with clean air upon advection.[8] V-SOA includes products from reactions of 51 measured VOC (23 aromatics, 13 alkenes and 15 alkanes; under high-NO_x conditions, when the reaction of RO_2 + NO dominates over RO_2 + HO_2 and RO_2 + RO_2) with reaction yields and gas-particle partitioning coefficients from ref 19 for all VOC except high-yield aromatics and isoprene, for which we use the parameterization from ref 20 (under high and low-NO_x conditions) and ref 21, respectively. We refer to semivolatile gas-phase species in equilibrium with the V-SOA as V-$SVOC_g$. Previously, V-SOA from aromatic low-NO_x products was characterized as "non-volatile".[20] Here those products are assigned a saturation concentration (c^*) of 0.1 $\mu g\ m^{-3}$, a value sufficiently low to keep them in the particle-phase in all of the chamber experiments.[20] Table S1 of the Supporting Information provides detailed V-SOA model parameters. To illustrate the variability of different current V-SOA models, we also present the V-SOA parameterization of ref 4 (under high and low-NO_x conditions), in which aging of semivolatile VOC products results in SOA yields from, e.g., toluene of ~100% after ~3 days. Details of the aging V-SOA parameterization are given in Table S2 of the Supporting Information.

SI-SOA is simulated using parameters from either ref 10 (Robinson or "ROB") or using the updated parameters from ref 22 (Grieshop or "GRI"). When compared to ROB, species in GRI have 2× lower gas-phase reactivity, 10× larger reduction in c^* of semivolatile species per oxidation step, 5.3× more oxygen added to the products, as well as lower ΔH_{vap}, and some differences in assumed MW. The initial volatility distributions are the same in both parameterizations. Details of both parametrizations are given in Table S3 of the Supporting Information. G-SOA is calculated to account for ~15% of the measured SOA in the urban area;[8] however, it is not modeled here due to unconstrained volatility and aging. The model primary and secondary semivolatile species are assumed to partition only to the POA and SOA phases, respectively, based on the findings of ref 23 who reported a lack of partitioning of α-pinene SOA to lubricating oil POA. Although research continues on the best partitioning assumption for multi-component OA,[23,24] it was shown previously that the model results are only weakly sensitive to it.[8] Model OA results are compared with MILAGRO observations.[18,25−28]

We evaluate the effect of gas-phase aging on SOA mass with realistic dilution, NO_x concentrations, and temperature. Lagrangian trajectories determined from altitude-controlled balloons released near Mexico City, aircraft intercepts of those trajectories, and chemical model result consistent with the aircraft intercepts[29] are used to constrain the average physical and chemical conditions during aging. An air parcel located inside the well-mixed boundary layer at the Mexico City surface (2.2 km amsl and 20.5 °C) and containing the species emitted and formed after ~1/3 day of oxidation as in previous urban simulation,[8] is assumed to be rapidly advected over the city at a constant altitude and temperature of ~3.5 km amsl (~1.3 km above Mexico City) and 12 °C, respectively, toward the Gulf of Mexico, as illustrated in Figure S2 of the Supporting Information. Model results are considered vs photochemical age, rather than actual time, to remove the visually confounding effect of the daily cycles on the species concentrations. Explicit inclusion of diurnal variations in the model yielded nearly identical results. A constant dilution rate of 6.12% per hour, consistent with the observations,[29] was used. OH and O_3 concentrations are fixed at the regional diurnal averages estimated from the aircraft measurements as 1.46×10^6 molecules cm^{-3} and 60 ppbv, respectively (C. Cantrell, NCAR, Pers. comm., 2008). Evolution of NO_x and HO_2 is interpolated based on simulations from the CBM-Z photochemical mechanism in the same lagrangian framework.[30,31] NO concentrations linearly decrease, reducing the fraction of aromatic peroxy radicals reacting via the high-NO_x channel from 0.995 at the start to 0.1 at the end of simulation. Dry/wet deposition and emissions are ignored, and the air parcel is decoupled from the surface soon after advection.

3. RESULTS AND DISCUSSION

3.1. Evolution of Aerosol and Gas-Phase Organic Species during Aging.

3.1.1. Results with Non-Aging V-SOA Plus SI-SOA. Figure 1 shows model OA and gaseous organic mass concentrations during three-day aging, normalized to an inert tracer CO in

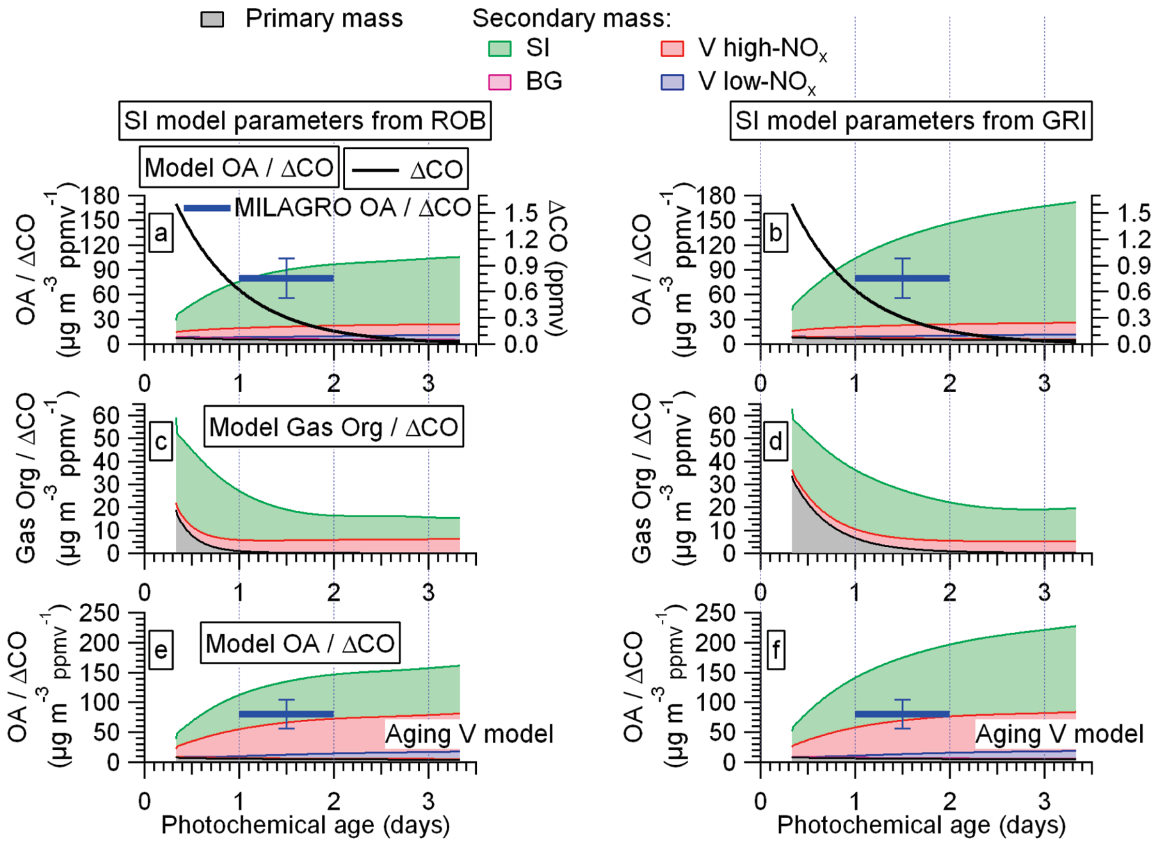

Figure 1. Evolution of total model OA during aging, normalized to ΔCO, for the ROB (left) and GRI (right) cases. (a,b): OA/ΔCO at STP conditions; (c,d): $SVOC_g$/ΔCO at STP conditions; (e,f): OA/ΔCO at STP when using the aging V model parameterization.[4] Model OA/ΔCO is compared to MILAGRO measurements after ∼2 days.[26]

excess to its background concentration of 0.1 ppmv (ΔCO) to remove the effect of dilution. SOA/ΔCO initially increases rapidly due to the high precursor concentrations, with the increase slowing down after ∼1.5 days due to the depletion of SOA precursors and some SOA evaporation upon dilution (Figure 1a, b). Comparison of model OA/ΔCO against MILAGRO observations for ∼2-day aged air masses [26] shows that OA/ΔCO for the ROB case matches the observations within the measurement uncertainties, while for the GRI case it is almost twice the observations, consistent with recent results of a 3D model that implemented these mechanisms for MILAGRO.[17] Total $SVOC_g$/ΔCO first decays quickly, primarily due to reaction of the primary and secondary $SIVOC_g$ (Figure 1c,d), becoming steady after ∼2 days. The low-NO_x V-SOA does not evaporate upon dilution under the conditions of this simulation, as its c^* (0.1 μg m^{-3}) is much lower than the minimum SOA concentration (∼2 μg m^{-3}); regardless, it is only ∼5% of total SOA (Figure S3a,c of the Supporting Information). Total SOA is initially ∼2/3 of total $SVOC_g$, while after three days total SOA accounts for ∼90% of secondary mass (Figure S3e−h of the Supporting Information).

V-SOA is initially dominated by high-NO_x aromatic products, but after 3 days of aging low-NO_x aromatic products make up ∼30% of V-SOA (Figure S4 of the Supporting Information). V-$SVOC_g$ is always dominated by high-NO_x products due to the low volatility of low-NO_x products. Other precursors besides high-yield aromatics only make minor contributions to V-SOA and V-$SVOC_g$, consistent with previous results.[8] Average volatility of secondary SI model species continuously decreases with photo-oxidation during aging (Figures S5 and S6 of the Supporting Information). This is enhanced by dilution, which leads to the evaporation of SI-SOA, oxidation of the evaporated species, and re-partitioning to the particle-phase, which increases the oxygen content of molecules, and thus the mass of SI-SOA. In terms of the initial P-$SIVOC_g$, aging increases the predominance of products from the initially more volatile yet overall more abundant IVOC (Figures S5 and S6 of the Supporting Information). For the ROB (GRI) case, the average secondary species underwent gas-phase oxidation only ∼2× (∼1×) at the start of the simulation, but ∼5× (∼2.5×) by the end (Figures S5 and S6 of the Supporting Information). The lower values for GRI result from its lower rate constant and larger decrease of volatility per-step.

3.1.2. Results with Aging V-SOA Plus SI-SOA. Results with the aging V model [4] are shown in Figure 1e,f, while Figure S7 of the Supporting Information shows the results of the simulations inside Mexico City for comparison with the results of ref 8. The aging V-SOA parameterization alone is able to match the observations; the addition of SI-SOA results in large overpredictions, as observed in ref 4. The aging V-SOA parameterization of ref 4 is not well constrained by laboratory observations. Therefore, in the remainder of this paper, we use the non-aging V model parametrization [19−21] as implemented in ref 8. Clearly there is a critical research need to reduce the uncertainties in V-SOA formation from VOC precursors under long aging times for further progress in SOA model evaluation.

3.1.3. Comparison with O/C Observations. O/C ratios for model OA are compared to MILAGRO ground and aircraft

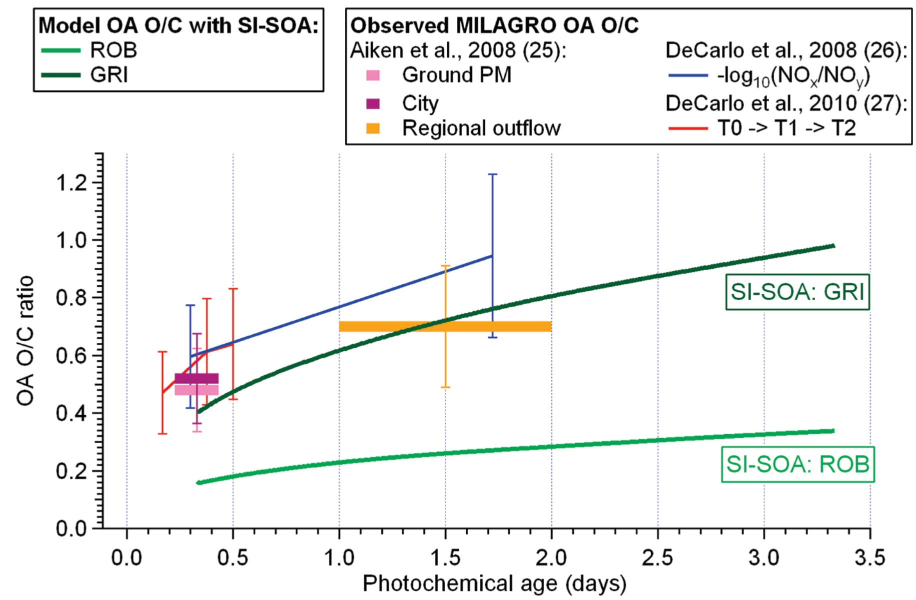

Figure 2. O/C atomic ratio for model OA for the ROB and GRI cases, compared to different estimates from the MILAGRO measurements.[25−27]

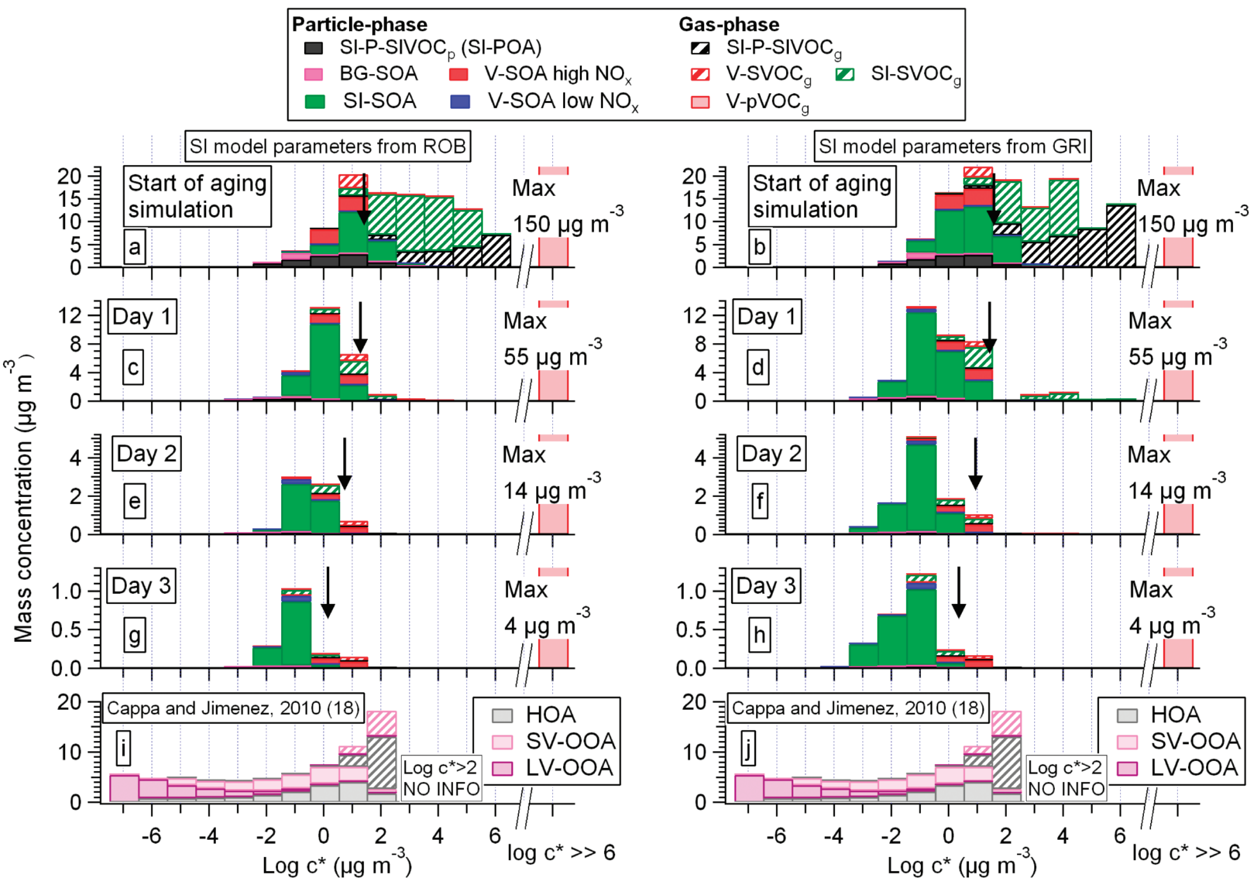

Figure 3. Volatility distribution of all model mass for the ROB (left) and GRI (right) cases at the start of aging simulation (a,b) and at the end of aging days one (c,d), two (e,f), and three (g,h). (i,j): The volatility distribution of SV-OOA, LV-OOA, HOA and their contributing gas-phase organics from ref 18. The downward pointing arrows represent the total SOA mass concentration at each point in time.

measurements [25−27] in Figure 2. The increase of model O/C with aging for GRI matches the observations, while for ROB it is much lower, again consistent with results from a regional model.[17]

Thus, we find the conflicting results: whereas ROB provides the best model-measurement agreement for SOA mass, GRI performs best in terms of OA O/C. Notably, we previously

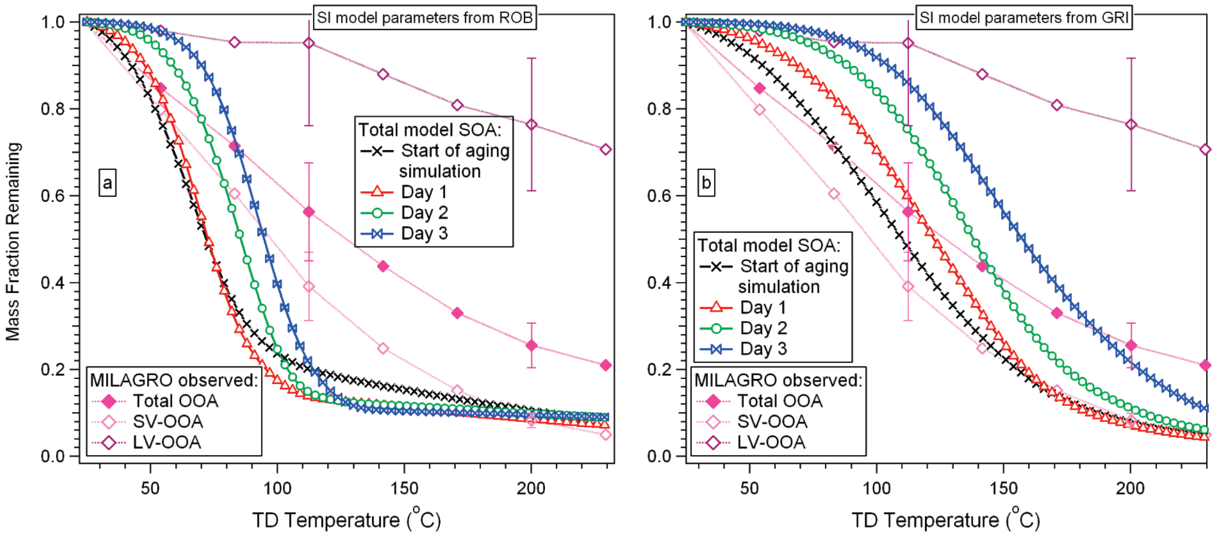

Figure 4. Fractional evaporation of total model SOA as a function of TD temperature assuming $\gamma = 0.1$ for the ROB (a) and GRI (b) cases, at the start of aging simulation and after three days of aging. Model results are compared to measurements during MILAGRO for total OOA and for its contributing SV-OOA and LV-OOA, which represent the expected range of measured volatilities, with representative error bars of ±20%.[28] MILAGRO observations are comparable with model results at the start of aging simulation (black).

demonstrated that at shorter aging time scales SOA mass and O/C closure can be obtained by adding G-SOA to ROB SI-SOA and V-SOA.[8]

3.2. Volatility of Model SOA.

3.2.1. Predicted Volatility Distributions. The evolution of the volatility of all model species during aging is shown in Figure 3. Total secondary mass at the start of simulations is nearly equally distributed between gas- and particle-phase. After one day most P-$SIVOC_g$ have reacted, greatly reducing the POA concentration through induced evaporation. $SVOC_g$ concentrations are much lower than at the start of the aging simulation, and most of the secondary products have $c^* \leq 10\ \mu g\ m^{-3}$. After two days SI-SOA species with $c^* \geq 1\ \mu g\ m^{-3}$ evaporate (due to dilution) and are oxidized, decreasing the volatility of SI model species. The final total model mass is characterized by the dominance of SOA over $SVOC_g$, and a continuous shift to lower volatilities, with nearly all model mass in volatility bins with $c^* \leq 1\ \mu g\ m^{-3}$. The differences between ROB and GRI appear small, with the most important one being the broader volatility distribution of GRI at the end of aging, while in ROB the distribution converges toward one bin. Figure 3 also shows a volatility distribution derived from thermal denuder (TD) measurements during MILAGRO,[18] which is comparable to those at the start of aging simulation. A clear difference is the lack of very low volatility material ($c^* < 0.01\ \mu g\ m^{-3}$) in the modeled volatility distributions, indicating that additional chemical pathways in the particle-phase (e.g., oligomerization) may be missing from the model.

3.2.2. Evaporation of Model SOA upon Heating. The evaporation of OA in downtown Mexico City was recently characterized using a TD + Aerodyne Aerosol Mass Spectrometer (TD-AMS) analysis.[18,28] We simulate the evaporation of total model SOA (V-SOA+SI-SOA) with a TD kinetic evaporation model.[8,18,32] We use an evaporation coefficient (γ) of 0.1 based on recent observations of slow evaporation of SOA (e.g., ref 33) that imply a kinetic limitation, and the results of ref 18 that showed that $\gamma \ll 0.1$ was inconsistent with the MILAGRO TD-AMS observations. Results using $\gamma = 1$ provide an upper-limit to the evaporation rate and are shown in Figures S8−S11 of the Supporting Information. The rest of the parameters are as described in ref 8. Because TD model results are highly sensitive to the ΔH_{vap} values used,[32] it is important to note that V model ΔH_{vap} is only 36 kJ mol^{-1} while somewhat larger values are used in the SI model (different between ROB and GRI).

Figure 4 shows TD evaporation of total model SOA, together with observations for fresh oxygenated OA ("semivolatile OOA" or SV-OOA), more aged OOA ("low volatility OOA" or LV-OOA), and total OOA in downtown Mexico City.[28] Note that according to the results of ref 18, OA that does not evaporate in the TD at ~100 °C is unlikely to evaporate under any atmospheric temperature or concentration conditions. Since volatility tends to decrease during aging,[18,28] the urban area observations likely represent an upper limit of the evaporation for more aged regional OOA. At the start of aging simulation, the volatility of total SOA for ROB is too high (Figure 4a) when compared to the urban OOA measurements, while GRI (Figure 4b) is closer to the observations. This difference is primarily due to lower ΔH_{vap} values in GRI than in ROB.[32] Continuous oxidation during aging produces more lower-volatility material, decreasing the overall model SOA volatility (Figure 4). Unfortunately no observations are available to quantitatively test the aged results. Due to the wider volatility distributions and lower ΔH_{vap} values, GRI yields smoother thermograms that more closely resemble the observations compared to ROB. The evaporation of SI- and V-SOA is shown in Figures S12 and S13 of the Supporting Information, respectively. For ROB the SI-SOA appears too volatile, while for GRI there is better agreement with measurements (Figure S12 of the Supporting Information). V-SOA shows lower evaporation than either SI-SOA case due to the low ΔH_{vap} of the V-SOA species (36 kJ mol^{-1}).[8] V-SOA during aging shows a strong trend toward slower evaporation (Figure S13 of the Supporting Information) due to the increased fraction of low-NO_x products. The evaporation of SI-POA (Figure S14 of the Supporting Information) is different than observed for hydrocarbon-like OA (HOA) in both cases. Overall TD model results are more strongly influenced by the specified ΔH_{vap} than by the volatility distribution, as illustrated in Figure S15 of the Supporting Information which shows that after swapping ΔH_{vap}

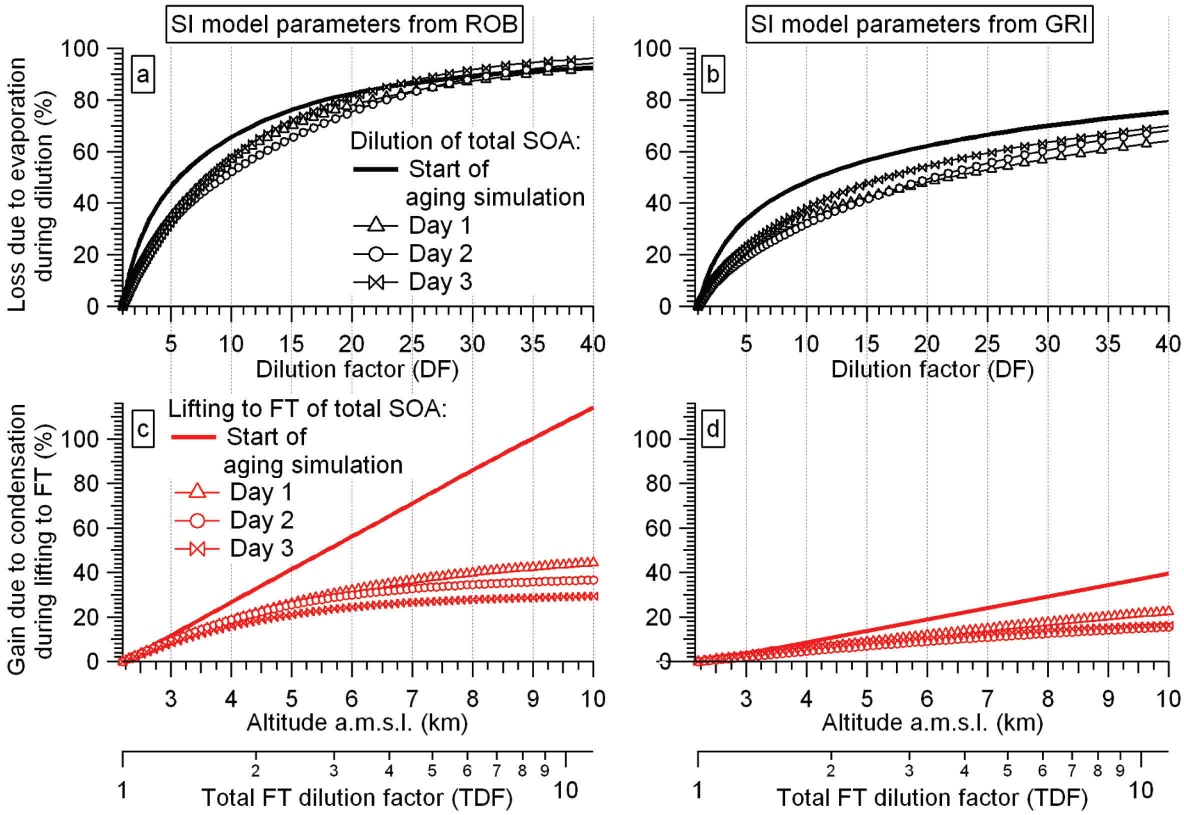

Figure 5. Fractional loss of total model SOA due to evaporation during dilution for the ROB and GRI cases (a and b, respectively) and fractional gain of total model SOA due to condensation upon rapid lifting to the FT during dry convection (c and d, respectively) for the start of aging simulation and after three days of aging. In c and d, model SOA is multiplied with a total dilution factor (TDF) that includes dilution due to: (i) changes in pressure and temperature; (ii) dilution during lifting to FT.

between ROB and GRI, the TD profile of ROB (GRI) using the alternate ΔH_{vap} strongly resemble the one of GRI (ROB) using the original ΔH_{vap} (Figure 4).

3.2.3. Influence of Dilution on Model SOA. SOA evaporation as polluted air is diluted with clean background is poorly characterized. To study this process, we isothermally dilute the model species and calculate the new equilibrium condition in the atmosphere for each day of aging (Figure 5a,b). For easier interpretation, the percent of OA mass lost due to evaporation, separate from the decrease of concentration due to dilution, is presented. This fractional loss is zero for completely non-volatile species, and > zero for semivolatile species. Total model SOA becomes somewhat less sensitive to dilution with initial aging and then remains stable: e.g., for the ROB case (Figure 5a), ~35% and ~50% of the initial and aged, respectively, SOA masses remain in the particle-phase for a dilution factor of 10. This reduction in evaporation results from the continued decrease in volatility of SI species and the fractional increase of less-volatile low-NO_x products in V-SOA. The GRI case shows lower evaporation due to its larger volatility decrease upon oxidation. The trends are similar for V-SOA and SI-SOA, when considered independently, while the dilution of SI-POA results in a strongly increased evaporation as the time progresses (Figure S16 of the Supporting Information).

3.2.4. Condensation upon Lifting of the Airmass. Cooling during the rise of an air parcel can lead to condensation of semivolatile $SVOC_g$ species as their saturation concentrations decrease, and this effect is important in producing enhanced SOA concentrations in the free troposphere (FT) in some models (e.g., ref 34). To evaluate this effect and how it would change with aging, we model the rapid lifting of SOA to the FT at the start of the aging simulation and at the end of each subsequent day of aging. The species present in the airmass are rapidly lifted to 10 km amsl without additional gas-phase oxidation and assuming no wet deposition. Each simulation ends at the altitude of 10 km amsl, and the lifted air is no longer considered in later simulations. From downtown Mexico City to 10 km amsl, the pressure and temperature are estimated to decrease from 775 hPa and 20.5 °C to 264 hPa and −30 °C. The factor by which the species concentrations (in μg m^{-3}) decrease due to the drop in pressure and temperature is calculated following the ideal gas law. This lofting decreases the species mass concentrations by ~60%, and the reduction in C_{OA} will additionally lead to some evaporation. However, a much stronger influence on C_{OA} is the decrease in temperature, which causes $SVOC_g$ to partition to the particle-phase.

It is expected that even for very fast lifting, the OA will undergo some additional dilution due to mixing with the clean background air. E.g. Cohan et al.[35] showed that CH_3I (a tracer for marine convection) was diluted ~4× by entrainment during convection from sea level to 10 km amsl, and approximately exponentially. Therefore, we assume that the dilution of the polluted air reduces the concentration of model species as $\exp\{-(h_{FT} - h_0)/H\}$, where h_0 is the initial height (2.2 and 3.5 km amsl for the start of aging simulation and three days of aging, respectively), h_{FT} is the height in FT, and H is estimated from ref 35 as 5 km. Note that the final reduction in concentration of model OA during rapid lifting to the FT could be much larger if wet deposition was active.

To focus only on the role of condensation, the SOA mass is normalized to the concentration of an inert tracer. The normalized total model SOA increases during lifting (Figure 5c,d). The change is the largest at the start of aging simulation when the initial $SVOC_g$ loadings that can condense upon lifting/cooling are highest (Figures 1 and 3). The $SVOC_g$ concentration decreases with aging, making the overall condensational growth progressively smaller. The effect is larger for the ROB than the GRI case, again due primarily to differences in their volatility basis-sets and ΔH_{vap}. The results for the individual model components are similar (Figure S17 of the Supporting Information).

Strong model SOA enhancement in the FT was previously reported and attributed to the condensation of secondary gaseous species during cooling (e.g., ref 34). To test this effect, we performed the same simulation of rapid lifting to FT as described above, but using only high-NO_x products of V model. Figure S18 of the Supporting Information shows that lifting to FT of those species after one day of aging will drastically increase V-SOA due to their high c^* and much lower starting C_{OA}. The same species will not form any V-SOA after aging days two and three due to too low C_{OA}.

4. IMPLICATIONS

Different combinations of SOA models presented here are capable of explaining different extensive (e.g., mass concentrations) and intensive (e.g., volatility and O/C ratio) SOA properties, yet we see that no single model currently captures all properties simultaneously. These results are highly relevant for regional and global SOA models, which may incorporate some of the mechanisms presented here. Processes not simulated here (e.g., oligomerization and water-phase chemistry) may also play important roles in SOA formation and aging. Therefore, this work highlights a critical need for additional research to characterize in more detail SOA, its precursors and their transformations and properties.

ASSOCIATED CONTENT

Supporting Information. Eighteen supporting figures. This material is available free of charge via the Internet at http://pubs.acs.org.

AUTHOR INFORMATION

Corresponding Author

*E-mail: jose.jimenez@colorado.edu.

Present Addresses

▽Particle Chemistry Department, Max Planck Institute for Chemistry, Mainz, Germany

¶Now a AAAS Science Policy Fellow at the U.S. EPA, Washington, DC

ACKNOWLEDGMENT

This research was supported by NSF (Grant ATM-0449815), DOE (BER, ASR Program, grant DE-FG02-08ER64627), and NOAA (Grant NA08OAR4310565). K.Dz. is grateful for fellowships from ASP-NCAR, ACD-NCAR and Dept. Chemistry and Biochemistry of Univ. of Colorado, and for funding from Particle Chemistry Department of Max Planck Institute for Chemistry. We thank A.C. Aiken and J.A. Huffman for providing data, and K. C. Barsanti, C. Cantrell, N.M. Donahue, J. Fast, A. Hodzic, J. Lee-Taylor, J.F. Pankow, and A.L. Robinson for many helpful discussions, and P. Hayes for help with manuscript preparation.

REFERENCES

(1) Zhang, Q.; et al. Ubiquity and dominance of oxygenated species in organic aerosols in anthropogenically-influenced Northern Hemisphere midlatitudes. *Geophys. Res. Lett.* **2007**, *34*, L13801, doi:13810.11029/12007GL029979.

(2) Hallquist, M.; et al. The formation, properties and impact of secondary organic aerosol: current and emerging issues. *Atmos. Chem. Phys.* **2009**, *9*, 5155–5235.

(3) Pankow, J. F. An absorption model of the gas/aerosol partitioning involved in the formation of secondary organic aerosol. *Atmos. Environ.* **1994**, *28*, 189–193.

(4) Tsimpidi, A. P.; et al. Evaluation of the volatility basis-set approach for the simulation of organic aerosol formation in the Mexico City metropolitan area. *Atmos. Chem. Phys.* **2010**, *10*, 525–546.

(5) Odum, J. R.; et al. Gas/particle partitioning and secondary organic aerosol yields. *Environ. Sci. Technol.* **1996**, *30*, 2580–2585.

(6) Donahue, N. M.; et al. Coupled partitioning, dilution, and chemical aging of semivolatile organics. *Environ. Sci. Technol.* **2006**, *40*, 2635–2643.

(7) Volkamer, R. M.; et al. Secondary organic aerosol formation from anthropogenic air pollution: Rapid and higher than expected. *Geophys. Res. Lett.*. **2006**, *33*, L17811, doi:10.1029/2006GL026899.

(8) Dzepina, K.; et al. Evaluation of recently-proposed secondary organic aerosol models for a case study in Mexico City. *Atmos. Chem. Phys.* **2009**, *9*, 5681–5709.

(9) Slowik, J. G.; et al. Characterization of a large biogenic secondary organic aerosol event from eastern Canadian forests. *Atmos. Chem. Phys.* **2010**, *10*, 2825–2845.

(10) Robinson, A. L.; et al. Rethinking Organic Aerosols: Semivolatile Emissions and Photochemical Aging. *Science* **2007**, *315*, 1259–1262.

(11) Volkamer, R. M.; et al. A missing sink for gas-phase glyoxal in Mexico City: Formation of secondary organic aerosol. *Geophys. Res. Lett.* **2007**, *34*, L19807, doi:10.1029/2007GL030752.

(12) Ervens, B.; Volkamer, R. M. Glyoxal processing by aerosol multiphase chemistry: Towards a kinetic modeling framework of secondary organic aerosol formation in aqueous particles. *Atmos. Chem. Phys.* **2010**, *10*, 8219–8244.

(13) Pandis, S. N.; et al. Secondary organic aerosol formation and transport. *Atmos. Environ.* **1992**, *26*, 2269–2282.

(14) Molina, L. T.; et al. An overview of the MILAGRO 2006 campaign: Mexico City emissions and their transport and transformation. *Atmos. Chem. Phys.* **2010**, *10*, 8697–8760.

(15) Kleinman, L. I.; et al. The time evolution of aerosol composition over the Mexico City plateau. *Atmos. Chem. Phys.* **2008**, *8*, 1559–1575.

(16) Hodzic, A.; et al. Modeling organic aerosols during MILAGRO: Importance of biogenic secondary organic aerosols. *Atmos. Chem. Phys.* **2009**, *9*, 6949–6981.

(17) Hodzic, A.; et al. Modeling organic aerosols in a megacity: potential contribution of semi-volatile and intermediate volatility primary organic compounds to secondary organic aerosol formation. *Atmos. Chem. Phys.* **2010**, *10*, 5491–5514.

(18) Cappa, C. D.; Jimenez, J. L. Quantitative estimates of the volatility of ambient organic aerosol. *Atmos. Chem. Phys.* **2010**, *10*, 5409–5424.

(19) Koo, B.; Ansari, A. S.; Pandis, S. N. Integrated approaches to modeling the organic and inorganic atmospheric aerosol components. *Atmos. Environ.* **2003**, *37*, 4757–4768.

(20) Ng, N. L.; et al. Secondary organic aerosol formation from *m*-xylene, toluene, and benzene. *Atmos. Chem. Phys.* **2007**, *7*, 3909–3922.

(21) Kroll, J. H.; et al. Secondary organic aerosol formation from isoprene photooxidation under high-NO_x conditions. *Geophys. Res. Lett.* **2005**, *32*, L18808, doi:10.1029/2005GL023637.

(22) Grieshop, A. P.; et al. Laboratory investigation of photochemical oxidation of organic aerosol from wood fires 1: Measurement and simulation of organic aerosol evolution. *Atmos. Chem. Phys.* **2009**, *9*, 1263–1277.

(23) Song, C.; et al. Effect of hydrophobic primary organic aerosols on secondary organic aerosol formation from ozonolysis of a-pinene. *Geophys. Res. Lett.* **2007**, *34*, L20803, doi:10.1029/2007GL030720.

(24) Asa-Awuku, A.; et al. Mixing and phase partitioning of primary and secondary organic aerosols. *Geophys. Res. Lett.* **2009**, *36*, L15827, doi:10.1029/2009GL039301.

(25) Aiken, A. C.; et al. O/C and OM/OC ratios of primary, secondary, and ambient organic aerosols with high resolution time-of-flight aerosol mass spectrometry. *Environ. Sci. Technol.* **2008**, *42*, 4478–4485.

(26) DeCarlo, P. F.; et al. Fast airborne aerosol size and chemistry measurements with the high resolution aerosol mass spectrometer during the MILAGRO campaign. *Atmos. Chem. Phys.* **2008**, *8*, 4027–4048.

(27) DeCarlo, P. F.; et al. Investigation of the sources and processing of organic aerosol over the Central Mexican Plateau from aircraft measurements during MILAGRO. *Atmos. Chem. Phys.* **2010**, *10*, 5257–5280.

(28) Huffman, J. A.; et al. Chemically-resolved aerosol volatility measurements from two megacity field studies. *Atmos. Chem. Phys.* **2009**, *9*, 7161–7182.

(29) Voss, P. B.; et al. Long-range pollution transport during the MILAGRO-2006 campaign: A case study of a major Mexico City outflow event using free-floating altitude-controlled balloons. *Atmos. Chem. Phys.* **2010**, *10*, 7137–7159.

(30) Zaveri, R. A.; Peters, L. K. A new lumped structure photochemical mechanism for large-scale applications. *J. Geophys. Res.* **1999**, *104*, 30387–30415.

(31) Zaveri, R. A.; et al. Ozone production efficiency and NO_x depletion in an urban plume: Interpretation of field observations and implications for evaluating O_3-NO_x-VOC sensitivity. *J. Geophys. Res.* **2003**, *108*, 4436, doi:10.1029/2002JD003144.

(32) Cappa, C. D. A model of aerosol evaporation kinetics in a thermodenuder. *Atmos. Meas. Tech.* **2010**, *3*, 579–592.

(33) Grieshop, A. P.; Donahue, N. M.; Robinson, A. L. Is the gas-particle partitioning in alpha-pinene secondary organic aerosol reversible? *Geophys. Res. Lett.* **2007**, *34*, L14810, doi:10.1029/2007GL029987.

(34) Kanakidou, M.; et al. Organic aerosol and global climate modelling: A review. *Atmos. Chem. Phys.* **2005**, *5*, 1053–1123.

(35) Cohan, D. S.; Schultz, M. G.; Jacob, D. J. Convective injection and photochemical decay of peroxides in the tropical upper troposphere: Methyl iodide as a tracer of marine convection. *J. Geophys. Res.* **1999**, *104* (D5), 5717–5724.

Modeling the Multiday Evolution and Aging of Secondary Organic Aerosol During MILAGRO 2006

Katja Dzepina[1,2,4 ‡], Christopher D. Cappa[5], Rainer M. Volkamer[1,2], Sasha Madronich[4], Peter F. DeCarlo[1,3‡‡,], Rahul A. Zaveri[6], and Jose L. Jimenez[1,2 *]

[1]Cooperative Institute for Research in Environmental Sciences, [2]Dept. Chemistry and Biochemistry, and [3]Dept. Atmospheric and Oceanic Sciences, Univ. of Colorado, Boulder, CO
[4] Atmospheric Chemistry Division, National Center for Atmospheric Research, Boulder, CO
[5]Dept. Civil and Environmental Engineering, Univ. Of California, Davis, CA
[6]Pacific Northwest National Laboratory, Richland, WA

[‡]Now at Max Planck Institute for Chemistry, Mainz, Germany
[‡‡]Now a AAAS Science Policy Fellow at the U.S. EPA, Washington, DC

* Corresponding author (email: jose.jimenez@colorado.edu)

Supporting Information Summary:

Number of SI pages: 13

Number of SI tables: 3

Number of SI figures: 18

Supporting Information Section

Section S1: List of abbreviations

Aging V model	Model for aging SOA formation from VOC. Uses parameterization from (4) for all species.
AMS	Aerodyne Aerosol Mass Spectrometer
BG-SOA	Background SOA
DF	Dilution factor used in simulations of model mass dilution
FT	Free troposphere
G-SOA	SOA from glyoxal
HOA	Hydrocarbon-like organic aerosols
IVOC	Intermediate volatility organic compounds
LV-OOA	Low volatility OOA
MCMA-2003	Mexico City Metropolitan Area 2003 field campaign
MILAGRO-2006	Megacity Initiative: Local and Global Research Observations 2006 field campaign
Non-aging V model	Model for non-aging SOA formation from VOC. In this work, parameterization from (19) is used for all VOC except for high-yield aromatics and isoprene, for which use parameterizations from (20) and (21), respectively, are used.
OA	Organic aerosols
OOA	Oxygenated organic aerosols

POA	Primary organic aerosols
P-SIVOC$_g$	Primary emitted gas-phase SIVOC
P-SIVOC$_{g+p}$	Total primary emitted SIVOC species in SI model; P-SIVOC$_{g+p}$ = P-SIVOC$_g$ + SI-POA
SI model	Model for SOA formation from semivolatile and intermediate volatility organic compounds (SIVOC). In this work, SI model parameterizations of (10) (Robinson or "ROB") and (22) (Grieshop or "GRI") are used.
SI-POA	POA emitted in SI model
SI-SOA	SOA formed in SI model
SI-SVOC$_g$	Secondary gas-phase species formed in SI model
SI-SVOC$_{g+p}$	Total secondary semivolatile (i.e. condensable) species formed in SI model; SI-SVOC$_{g+p}$ = SI-SOA + SI-SVOC$_g$
SIVOC	Semivolatile and intermediate volatility organic compounds
SOA	Secondary organic aerosols
SVOC	Semivolatile organic compounds
SV-OOA	Semivolatile OOA
TDF	Total dilution factor used in simulations of rapid lifting to FT. TDF is composed of contributions from: i) ideal gas law, as $F_{FT} = (T_0/T_{FT}) * (P_{FT}/P_0)$, where $T_0(P_0)$ and T_{FT} (P_{FT}) are the temperatures (pressures) at surface and during lifting to FT, respectively; and ii) dilution during rapid lifting to FT, as $\exp\{-(h_{FT}–h_0)/H\}$, where h_0 is the initial

	height (2.2 km amsl), h_{FT} is the height in FT, and H is estimated from (35) as 5 km.
VOC	Volatile organic compounds
V-pVOC	Secondary product VOC formed in V model
V-SOA	SOA formed in V model
V-$SVOC_g$	Secondary gas-phase species formed in V model
V-$SVOC_{g+p}$	Total semivolatile (i.e. condensable) species formed in V model; V-$SVOC_{g+p}$ = V-SOA + V-$SVOC_g$

Table S1: Speciation and assumptions of non-aging V model parameterization adapted from (19) and (20). Table S1 is identical to Table SI-1 of (8), with the exception of non-zero *c** values of isoprene and low-NO_x channel products.

Lumped precursor species name	**Measured precursor species**	k_{OH} (k_{O3}) **(cm^3 molec^{-1} s^{-1})**	**Stoichiometric SOA yield, *α* (dimensionless)**	***c**** **(300 K) (μg m^{-3})**
One-product precursors				
AAR3	Methylcyclopentane Cyclohexane Methylcyclohexane C7-Cycloparaffins n-Heptane, Heptanes isomers n-Octane, Octane isomers n-Nonane, Nonane isomers	8.43×10^{-12}	0.004	1.35
AAR4	>C8-Cycloparaffins n-Decane, Decane isomers Undecane isomers >C12-isomers	1.23×10^{-11}	0.014	1.80
OLE1	Propene 1-Butene 1-Pentene, 1-Pentene isomers 1-Hexene isomers	3.16×10^{-11} (8.92×10^{-18})	0.002	0.90
OLE3	1,3-Butadiene 2-Pentene isomers 2-Hexene isomers Cyclopentene >=Cyclohexene	6.59×10^{-11} (1.21×10^{-16})	0.004	1.12
C7OL	Heptene isomers	6.34×10^{-11} (1.15×10^{-16})	0.013	1.35
C8OL	Octene isomers	6.34×10^{-11} (1.15×10^{-16})	0.035	1.58

Lumped precursor species name	**Measured precursor species**	k_{OH} (k_{O3}) **(cm^3 molec^{-1} s^{-1})**	**Stoichiometric SOA yield, α (dimensionless)**	**c^* (300 K) (µg m^{-3})**
One-product precursors – cont.				
C9OL	Nonene isomers	6.34×10^{-11} (1.15×10^{-16})	0.044	1. 58
PHEN	Phenol	1.63×10-11	0.031	1.35
BALD	Benzaldehyde Aromatic aldehydes	1.15×10^{-11}	0.0008	1. 58
CRES	Cresols	4.1×10^{-11}	0.034	1.58
ISOP[1]	Isoprene	1.02×10^{-10} (1.28×10^{-17})	0.015	0.1
Two-products precursors				
TERP	Terpenes	5.37×10^{-11} (8.52×10^{-17})	High-NO$_x$ P1: 0.038 High-NO$_x$ P2: 0.326	3.35 143.2
ARO1[2]	i) Toluene ii) Ethylbenzene i-, n-Propylbenzene i-Butylbenzene o-, m-, p-Ethyltoluene Diethylbenzene isomers	i) 5.96×10^{-12} ii) 9.57×10^{-12};	High-NO$_x$ P1: 0.058 High-NO$_x$ P2: 0.113 Low-NO$_x$: 0.36	2.54 23.28 0.1
BENZ	Benzene	1.23×10^{-12}	High-NO$_x$ P1: 0.072 High-NO$_x$ P2: 0.888 Low-NO$_x$: 0.37	0.33 121.63 0.1
ARO2[2]	i) 1,2,3-, 1,2,4-, 1,3,5-Trimethylbenzene ii) m-xylene iii) p-xylene iv) Styrene v) Naphthalene Methylnaphthalene isomers Other naphthalenes	i) 4.32×10^{-11}; ii) 2.36×10^{-11}; iii) 1.43×10^{-11}; iv) 5.20×10^{-11}; v) 2.30×10^{-11}	High-NO$_x$ P1: 0.031 High-NO$_x$ P2: 0.09 Low-NO$_x$: 0.30	1.44 39.47 0.1

ΔH_{vap} for all SOA products, except low-NO_x SOA products, is 36 kJ mol^{-1} (Volkamer et al., 2006).

[1]Isoprene aerosol yields are adopted from (21).

[2]ARO1 and ARO2 are defined after original (19) lumping as AAR5 + toluene, and AAR6 + AAR7, respectively.

Table S2: Speciation and assumptions of aging V model parameterization adapted from (4). The SOA yields are based on an assumed density of 1.5 g cm^{-3}. All gas-phase species react with k_{OH} = 1 x 10^{-11} cm^{3} molec^{-1} s^{-1}. Note that the aging rate constant was erroneously reported as 4 x 10^{-11} cm^{3} molec^{-1} s^{-1} in (4), while the actual rate constant used was 1 x 10^{-11} cm^{3} molec^{-1} s^{-1}.

Lumped precursor species name	**Measured precursor species**	**Stoichiometric SOA yield, *α* (dimensionless) for species with *c** at 298 K (μg m^{-3}):**								**Molecular weight (g mol^{-1})**
		1	**10**	**100**	**1000**	**1**	**10**	**100**	**1000**	
		High-NO$_x$ parameterization				**Low-NO$_x$ parameterization**				
ALK4	n-Pentane, n-Hexane, Branched C5-C6 Alkanes, Cyclopetane, Trimethyl Butane, Trimethyl Pentane, Isopropyl alcohol, n-Propyl Alcohol	0.000	0.038	0.000	0.000	0.000	0.075	0.000	0.000	120
ALK5	C7-C22 n-Alkanes, C6-C16 Cycloalkanes, Branched/Unspeciated C8-C18 Alkanes	0.000	0.015	0.000	0.000	0.000	0.300	0.000	0.000	150
OLE1	Propene, C4-C15 Terminal Alkenes	0.001	0.005	0.038	0.150	0.005	0.009	0.060	0.225	120
OLE2	Isobutene, C4-C15 Internal Alkenes, C6-C15 Cyclic or di-olefins, Styrenes	0.003	0.026	0.083	0.270	0.023	0.044	0.129	0.375	120
ARO1	Toluene, Benzene, Ethyl Benzene, C9-C13 Monosubstituted Benzenes	0.003	0.165	0.300	0.435	0.075	0.225	0.375	0.525	150
ARO2	Xylenes, Ethyl Toluenes, Dimethyl and Trimethyl Benzenes, Ethylbenzenes, Naphthalene, C8-C13 Di-, Tri-, Tetra-, Penta-, Hexa-substituted Benzenes, Unspeciated C10-C12 Aromatics	0.002	0.195	0.300	0.435	0.075	0.300	0.375	0.525	150
ISOP	Isoprene	0.001	0.023	0.015	0.000	0.009	0.030	0.015	0.000	136
TERP	α-pinene, β-pinene, Limonene, Carene, Sabinene, Other monoterpenes	0.012	0.122	0.201	0.500	0.107	0.092	0.359	0.600	180

Table S3: Comparison of SI model parameterizations for ROB and GRI cases (adopted from (10) and (22), respectively).

P-SIVOC$_{g+p}$ from initial lumped bin	**c^* (@ 300 K) (μg m^{-3})**	**ΔH_{vap} (kJ mol^{-1})**		**Molecular weight (g mol^{-1})**		**Fraction in total of P-SIVOC$_{g+p}$ from initial lumped bin (%)**
ROB and GRI	ROB and GRI	ROB	GRI	ROB	GRI	ROB and GRI
P-SIVOC$_{1,g+p}$	0.01	112	77	250	524	1.2
P-SIVOC$_{2,g+p}$	0.1	106	73	250	479	2.4
P-SIVOC$_{3,g+p}$	1	100	69	250	434	3.6
P-SIVOC$_{4,g+p}$	10	94	65	250	389	5.6
P-SIVOC$_{5,g+p}$	100	88	61	250	344	7.2
P-SIVOC$_{6,g+p}$	1000	82	57	250	299	12
P-SIVOC$_{7,g+p}$	10000	76	54	250	254	16
P-SIVOC$_{8,g+p}$	100000	70	50	250	208	20
P-SIVOC$_{9,g+p}$	1000000	64	46	250	163	32

	ROB	GRI
k(OH) (cm^3 molec^{-1} s^{-1}) at 300 K	4×10^{-11}	2×10^{-11}
Oxygen gain per oxidation generation	1.075	1.4
Volatility bin shift per oxidation generation	1	2

Supporting Information Figure Captions

Figure S1: Mechanisms and partitioning scheme used in this work. See text for details.

Figure S2: The conceptual framework of this work, in which an air parcel is rapidly advected from Mexico City surface (2.2 km amsl) to 3.5 km amsl towards the Gulf of Mexico. See text for details.

Figure S3: Evolution of total model mass during aging for the ROB (left) and GRI (left) cases. (a, c): fraction of OA; (b, d): fraction of $SVOC_g$; (e, g): mass concentrations of particle-phase model species; (f, h): mass concentrations of gas-phase model species.

Figure S4: Speciation of V-SOA (left) and V-$SVOC_g$ (right) during aging. (a, b): mass concentrations of V model species; (c, d): fraction of V model species; (e): V-SOA/ΔCO ratio at STP conditions; (f): V-$SVOC_g$/ΔCO ratio at STP conditions.

Figure S5: Speciation of SI-SOA (left) and SI-$SVOC_g$ (right) for ROB during aging. (a, b): mass concentrations of secondary SI model species divided by their $c*$; (c, d): fraction of secondary SI model species divided by their $c*$; (e, f): fraction of secondary SI model species from initial P-$SIVOC_{g+p}$ lumped volatility bin; (g, h): fraction of secondary SI model species divided by the number of generations of oxidation. See Table 2 in (8) for the detailed explanation of categories.

Figure S6: Speciation of SI-SOA (left) and SI-$SVOC_g$ (right) for GRI during aging. (a, b): mass concentrations of secondary SI model species divided by their $c*$; (c, d): fraction of secondary SI model species divided by their $c*$; (e, f): fraction of secondary SI model species from initial P-$SIVOC_{g+p}$ lumped volatility bin; (g, h): fraction of secondary SI model species divided by the number of generations of oxidation. See Table 2 in (8) for the detailed explanation of categories.

Figure S7: Evolution of total model SOA at the ground inside Mexico City compared to OOA measurements for: (a) the case study of (8) with non-aging V-SOA + ROB case SI-SOA; (b):

with non-aging V-SOA + GRI case SI-SOA; (c): with aging V-SOA + ROB case SI-SOA; and (d): with aging V-SOA + GRI case SI-SOA.

Figure S8: Fractional evaporation of total model SOA as a function of TD temperature assuming $\gamma=1$ for the ROB (a) and GRI (b) cases, at the start of aging simulation and after three days of aging. Model results are compared to measurements during MILAGRO for total OOA and for its contributing SV-OOA and LV-OOA, which represent the expected range of measured volatilities, with representative error bars of ±20% (28). MILAGRO observations are comparable with model results at the start of aging simulation (black).

Figure S9: Fractional evaporation of SI-SOA as a function of TD temperature assuming $\gamma=1$ for the ROB (a) and GRI (b) cases, at the start of aging simulation and after three days of aging. Model results are compared to measurements during MILAGRO for total OOA and for its contributing SV-OOA and LV-OOA, which represent the expected range of measured volatilities, with representative error bars of ±20% (28). MILAGRO observations are comparable with model results at the start of aging simulation (black).

Figure S10: Fractional evaporation of V-SOA as a function of TD temperature assuming $\gamma=1$ for the ROB (a) and GRI (b) cases, at the start of aging simulation and after three days of aging. Model results are compared to measurements during MILAGRO for total OOA and for its contributing SV-OOA and LV-OOA, which represent the expected range of measured volatilities, with representative error bars of ±20% (28). MILAGRO observations are comparable with model results at the start of aging simulation (black).

Figure S11: Fractional evaporation of SI-POA as a function of TD temperature assuming $\gamma=1$ for the ROB (a) and GRI (b) cases, at the start of aging simulation and after three days of aging. Model results are compared to measurements during MILAGRO for HOA, as well as for total

OOA and for its contributing SV-OOA and LV-OOA, which represent the expected range of measured volatilities, with representative error bars of ±20% (28). MILAGRO observations are comparable with model results at the start of aging simulation (black).

Figure S12: Fractional evaporation of SI-SOA as a function of TD temperature assuming γ=0.1 for the ROB (a) and GRI (b) cases, at the start of aging simulation and after three days of aging. Model results are compared to measurements during MILAGRO for total OOA and for its contributing SV-OOA and LV-OOA, which represent the expected range of measured volatilities, with representative error bars of ±20% (28). MILAGRO observations are comparable with model results at the start of aging simulation (black).

Figure S13: Fractional evaporation of V-SOA as a function of TD temperature assuming γ=0.1 for the ROB (a) and GRI (b) cases, at the start of aging simulation and after three days of aging. Model results are compared to measurements during MILAGRO for total OOA and for its contributing SV-OOA and LV-OOA, which represent the expected range of measured volatilities, with representative error bars of ±20% (28). MILAGRO observations are comparable with model results at the start of aging simulation (black).

Figure S14: Fractional evaporation of SI-POA as a function of TD temperature assuming γ=0.1 for the ROB (a) and GRI (b) cases, at the start of aging simulation and after three days of aging. Model results are compared to measurements during MILAGRO for HOA, as well as for total OOA and for its contributing SV-OOA and LV-OOA, which represent the expected range of measured volatilities, with representative error bars of ±20% (28). MILAGRO observations are comparable with model results at the start of aging simulation (black).

Figure S15: Influence of changing ΔH_{vap} values on calculated fractional evaporation of total model SOA as a function of TD temperature assuming an evaporation coefficient of 0.1 for the

ROB (a) and GRI (b) cases, at the start of the aging simulation and after three days of aging. The volatility of total model SOA in which *ΔH_{vap}* are replaced between ROB and GRI, while keeping all other ROB and GRI parameters the same, are compared to those presented in Figure 4.

Figure S16: Fractional loss due to evaporation during dilution for the ROB (left) and GRI (right) cases at the start of aging simulation and after each of three days of aging for: (a, b) V-SOA; (c, d): SI-SOA; and (e, f): SI-POA.

Figure S17: Fractional gain due to condensation upon rapid lifting to the free troposphere (FT) during dry convection for the ROB (left) and GRI (right) cases at the start of aging simulation and after each of three days of aging for: (a,b):V-SOA; (c, d): SI-SOA; and (e, f): SI-POA. Model mass is multiplied with total dilution factor (TDF) that includes dilution due to: i) changes in pressure and temperature, and ii) dilution during lifting to FT.

Figure S18: Fractional gain due to condensation upon rapid lifting to the free troposphere (FT) for only high-NO_x channel V-SOA products at the start of aging simulation and after each of three days of aging. Model mass is multiplied with total dilution factor (TDF) that includes dilution due to: i) changes in pressure and temperature, and ii) dilution during lifting to FT.

Supplementary Info Figures

Modeling the Multiday Evolution and Aging of Secondary Organic Aerosol During MILAGRO 2006

Katja Dzepina, Christopher D. Cappa, Rainer M. Volkamer, Sasha Madronich, Peter F. DeCarlo,, Rahul A. Zaveri, and Jose L. Jimenez

Correspondence author: jose.jimenez@colorado.edu

Figure S1

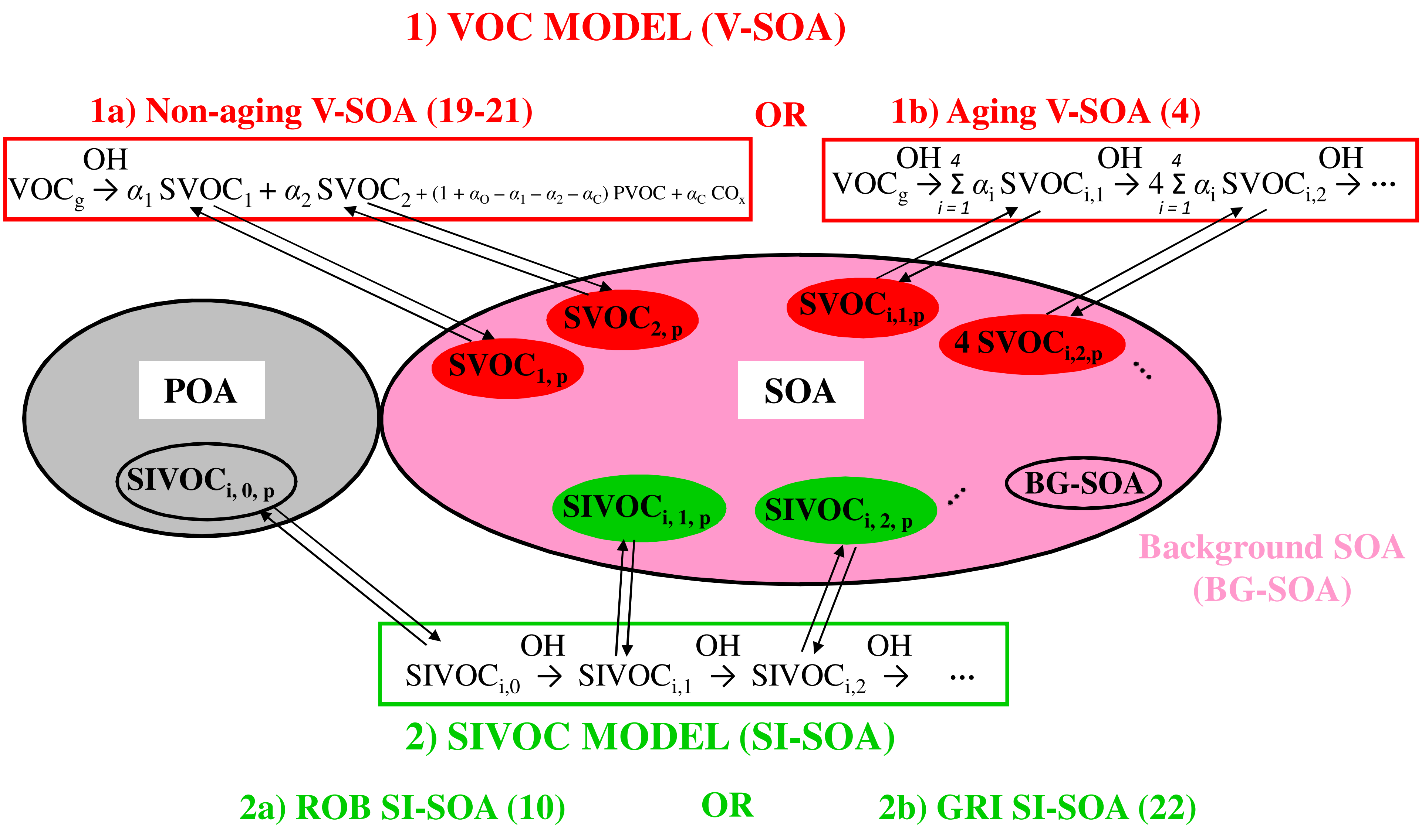

1) VOC MODEL (V-SOA)
1a) Non-aging V-SOA (19-21)
OR
1b) Aging V-SOA (4)
OH
VOC_g → α_1 SVOC_1 + α_2 SVOC_2 + (1 + α_O − α_1 − α_2 − α_C) PVOC + α_C CO_x
OH OH OH
VOC_g → Σ_{i=1}^{4} α_i SVOC_{i,1} → 4 Σ_{i=1}^{4} α_i SVOC_{i,2} → …
SVOC_{2, p}
SVOC_{1, p}
SVOC_{i,1,p}
4 SVOC_{i,2,p}
POA
SOA
SIVOC_{i, 0, p}
SIVOC_{i, 1, p}
SIVOC_{i, 2, p}
BG-SOA
Background SOA (BG-SOA)
OH OH OH
SIVOC_{i,0} → SIVOC_{i,1} → SIVOC_{i,2} → …
2) SIVOC MODEL (SI-SOA)
2a) ROB SI-SOA (10)
OR
2b) GRI SI-SOA (22)

Figure S2

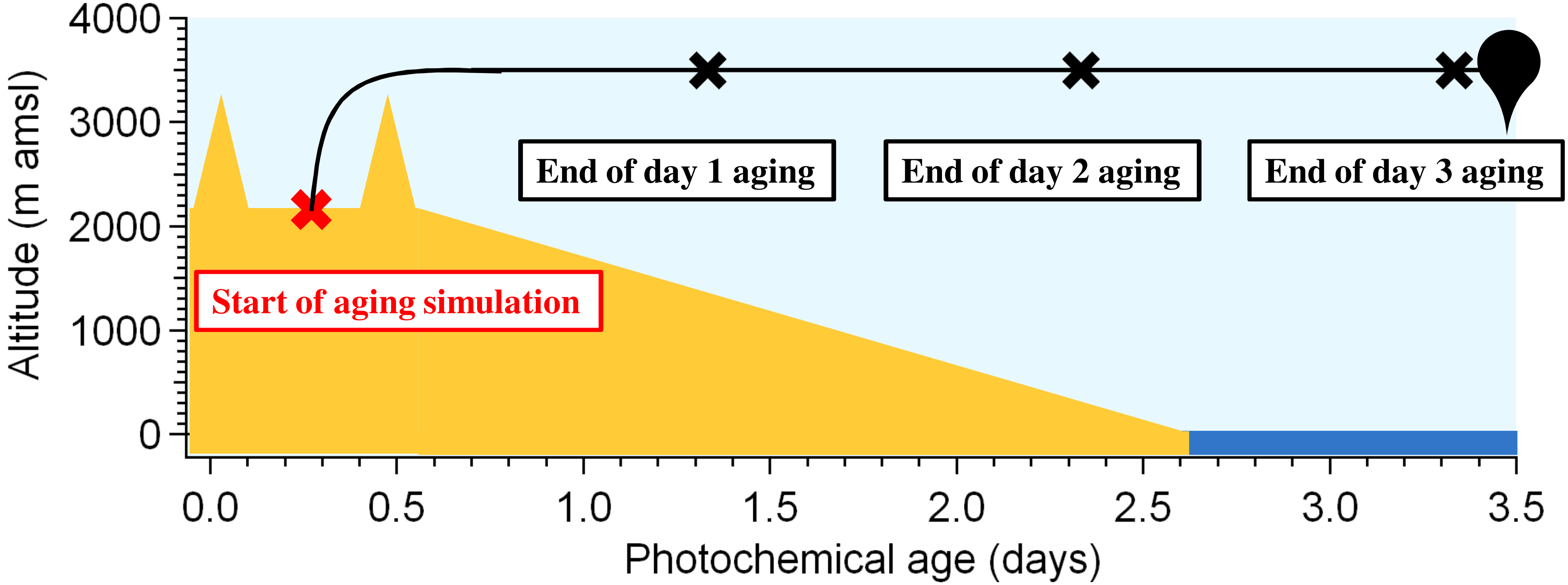

4000
3000
2000
1000
0
Altitude (m amsl)
End of day 1 aging
End of day 2 aging
End of day 3 aging
Start of aging simulation
0.0
0.5
1.0
1.5
2.0
2.5
3.0
3.5
Photochemical age (days)

Figure S3

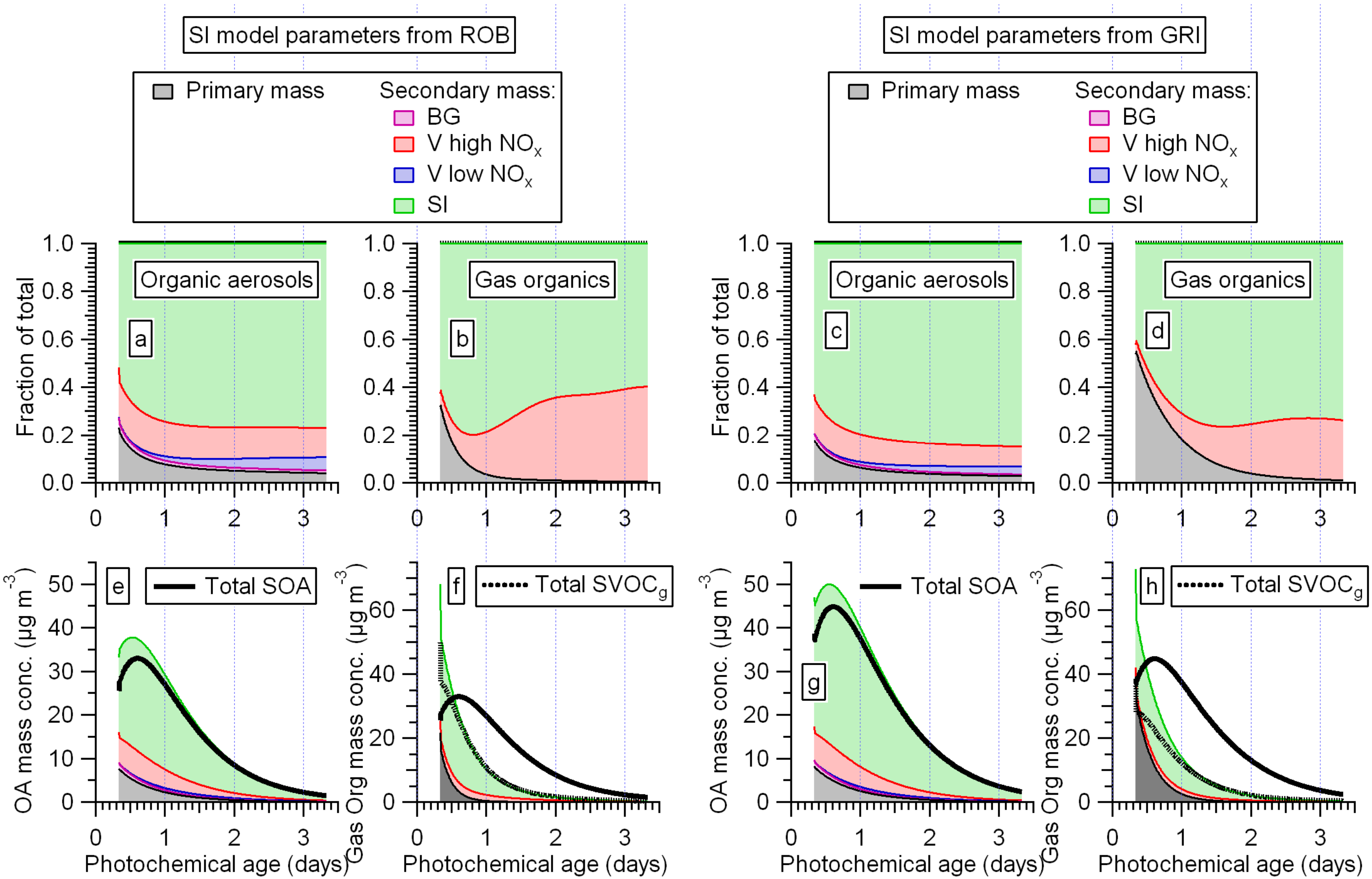

SI model parameters from ROB
SI model parameters from GRI
Primary mass
Secondary mass:
BG
V high NOx
V low NOx
SI
Organic aerosols
Gas organics
a
b
c
d
e
f
g
h
Fraction of total
Total SOA
Total SVOCg
OA mass conc. (µg m-3)
Gas Org mass conc. (µg m-3)
Photochemical age (days)

Figure S4

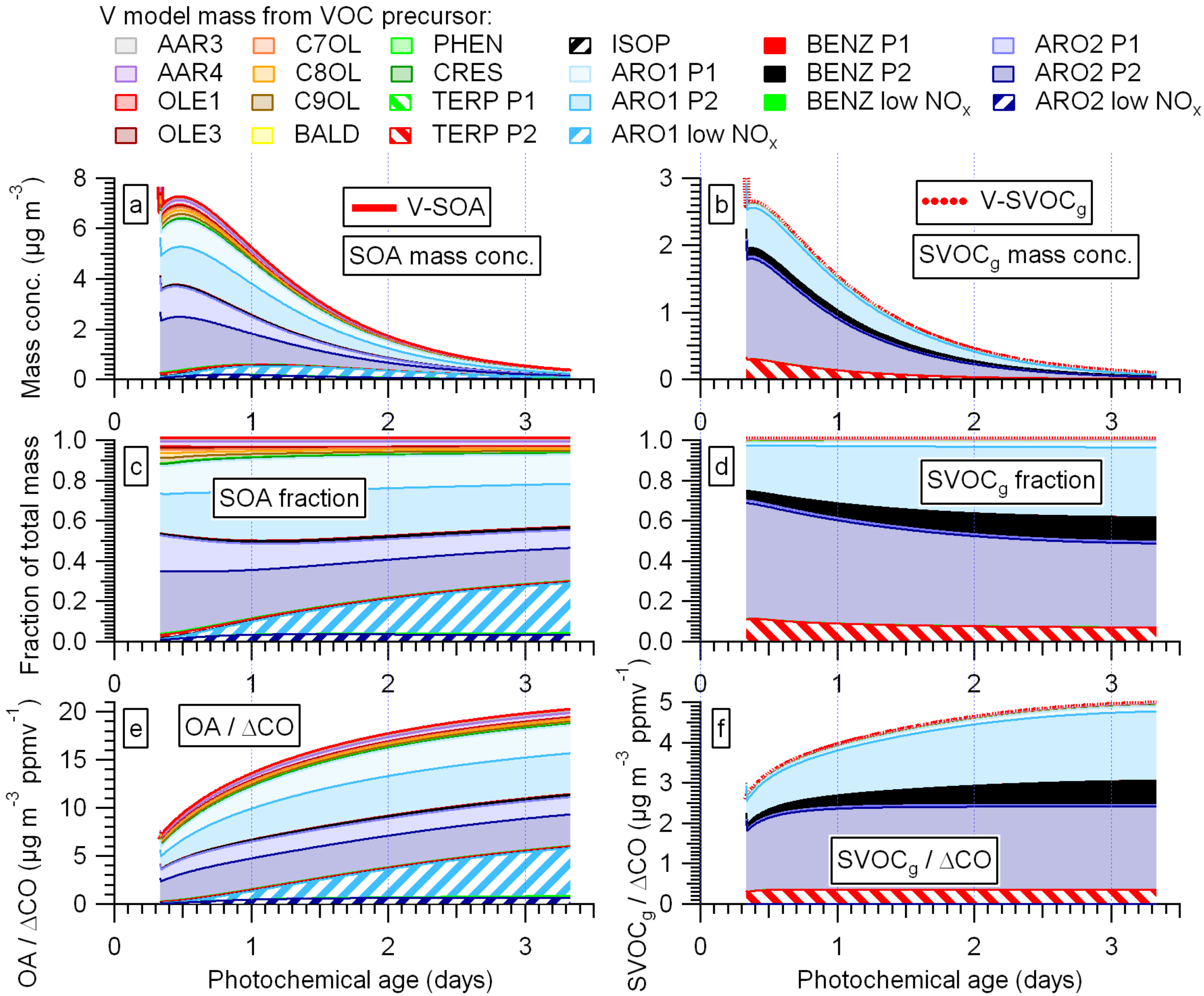

V model mass from VOC precursor:
AAR3
AAR4
OLE1
OLE3
C7OL
C8OL
C9OL
BALD
PHEN
CRES
TERP P1
TERP P2
ISOP
ARO1 P1
ARO1 P2
ARO1 low NOx
BENZ P1
BENZ P2
BENZ low NOx
ARO2 P1
ARO2 P2
ARO2 low NOx
a
V-SOA
SOA mass conc.
Mass conc. (μg m-3)
b
V-SVOCg
SVOCg mass conc.
c
SOA fraction
Fraction of total mass
d
SVOCg fraction
e
OA / ΔCO
OA / ΔCO (μg m-3 ppmv-1)
f
SVOCg / ΔCO
SVOCg / ΔCO (μg m-3 ppmv-1)
Photochemical age (days)
Photochemical age (days)

Figure S5

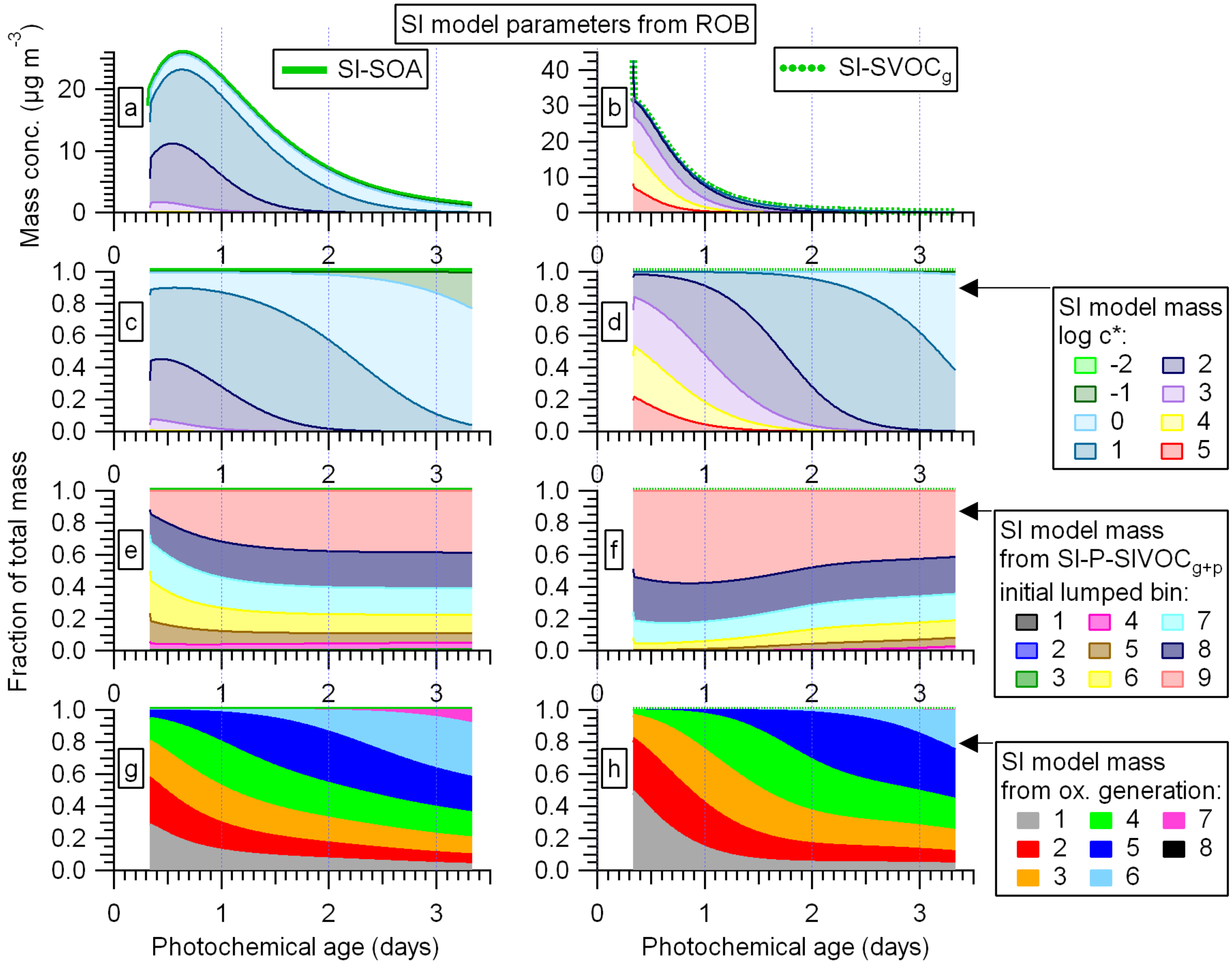

SI model parameters from ROB
SI-SOA
SI-SVOC$_g$
Mass conc. (µg m^{-3})
Fraction of total mass
a
b
c
d
e
f
g
h
SI model mass log c*:
-2
-1
0
1
2
3
4
5
SI model mass from SI-P-SIVOC$_{g+p}$ initial lumped bin:
1
2
3
4
5
6
7
8
9
SI model mass from ox. generation:
1
2
3
4
5
6
7
8
Photochemical age (days)
Photochemical age (days)

Figure S6

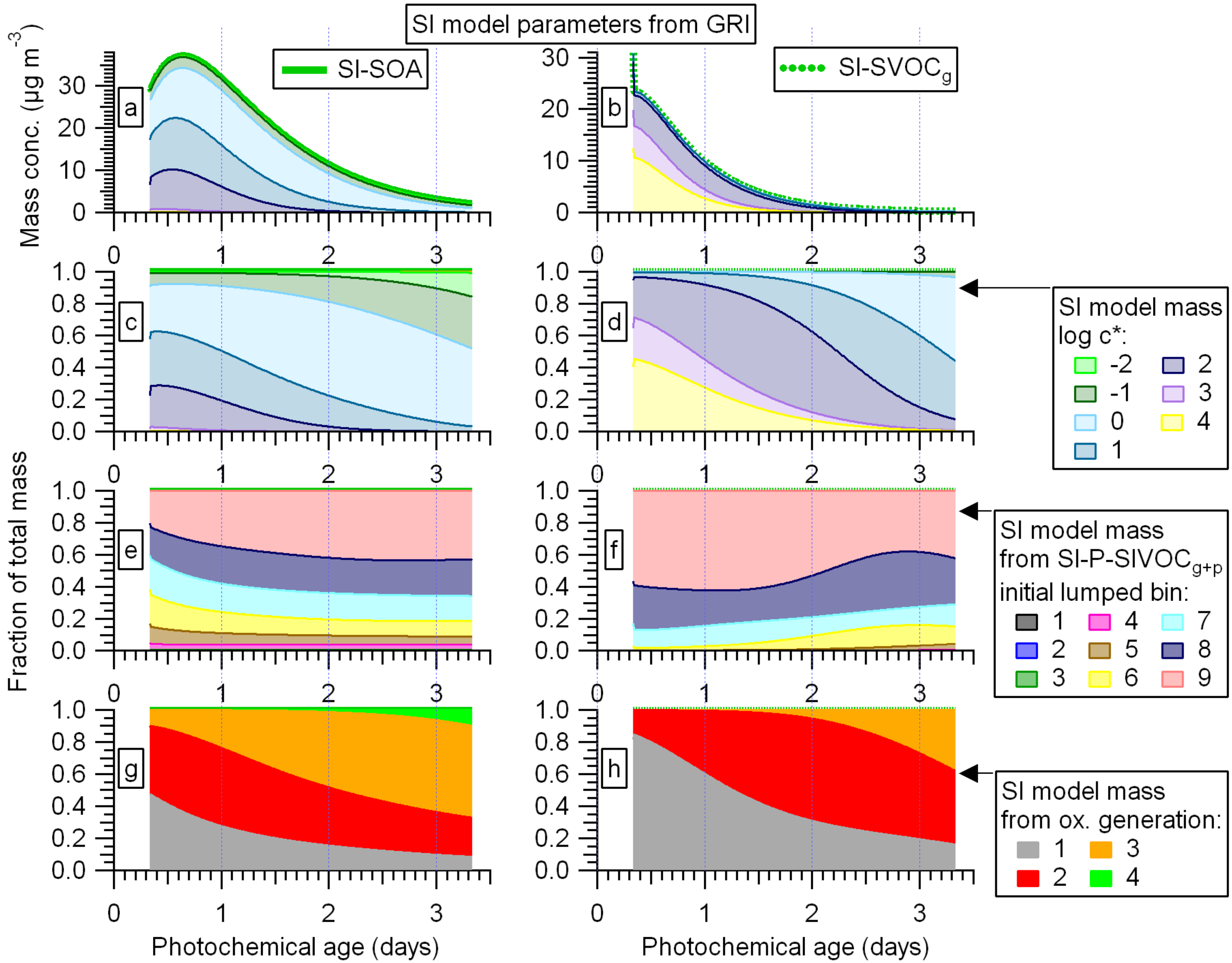

SI model parameters from GRI
SI-SOA
SI-SVOC$_g$
Mass conc. (μg m^{-3})
Fraction of total mass
a
b
c
d
e
f
g
h
SI model mass log c*:
-2
-1
0
1
2
3
4
SI model mass from SI-P-SIVOC$_{g+p}$ initial lumped bin:
1 2 3 4 5 6 7 8 9
SI model mass from ox. generation:
1 2 3 4
Photochemical age (days)
Photochemical age (days)

Figure S7

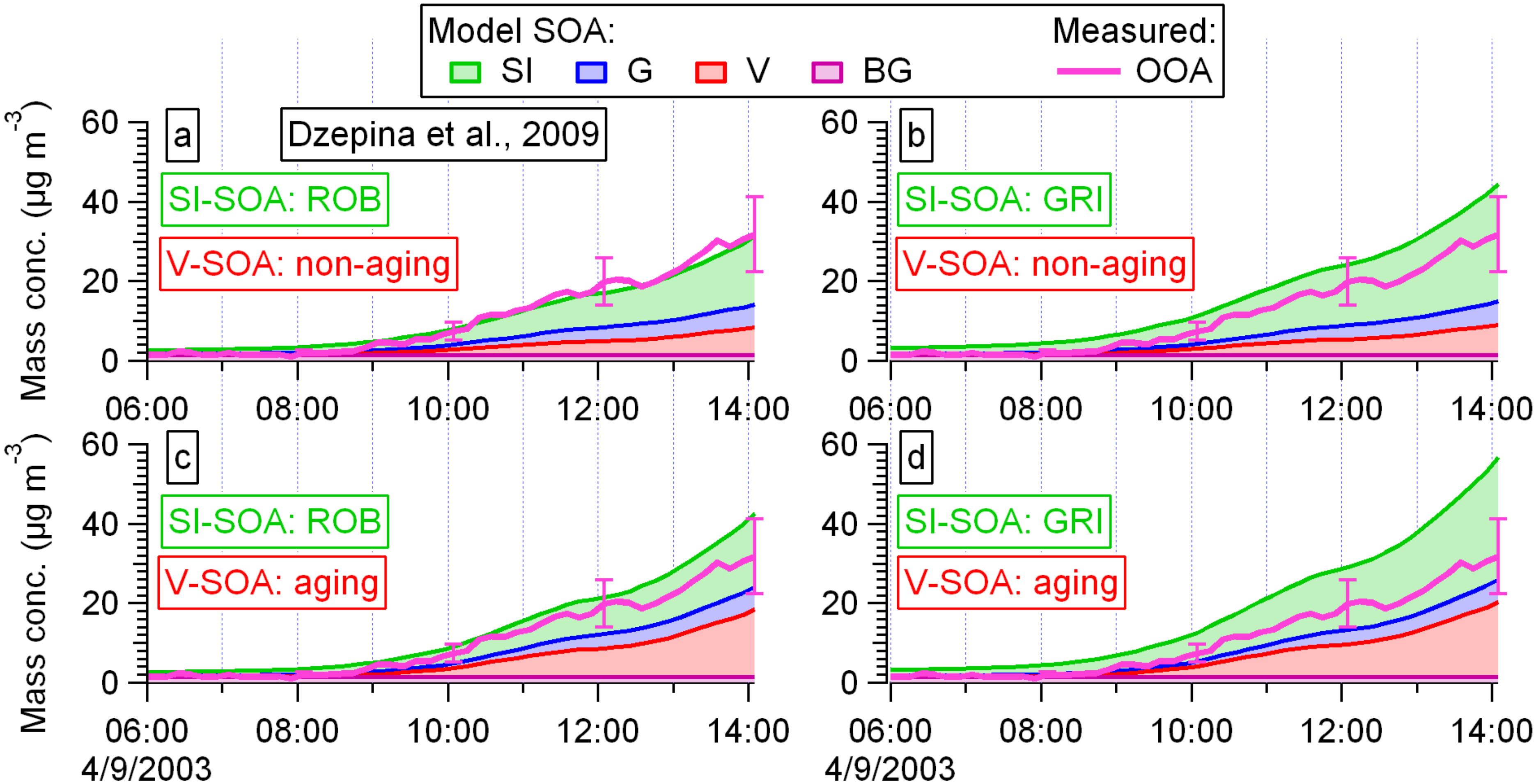

Model SOA:
SI
G
V
BG
Measured:
OOA
a
Dzepina et al., 2009
SI-SOA: ROB
V-SOA: non-aging
b
SI-SOA: GRI
V-SOA: non-aging
c
SI-SOA: ROB
V-SOA: aging
d
SI-SOA: GRI
V-SOA: aging
Mass conc. (µg m-3)
0
20
40
60
06:00
08:00
10:00
12:00
14:00
4/9/2003

Figure S8

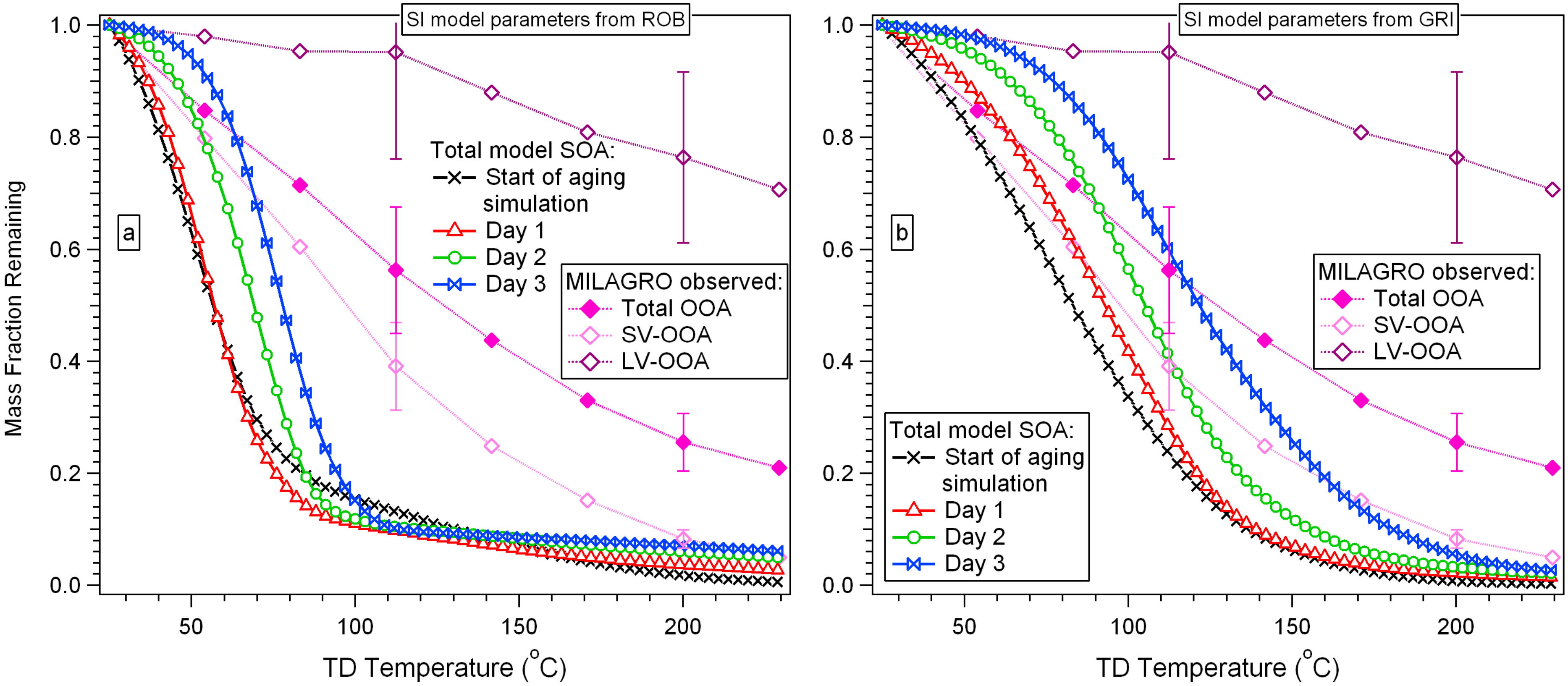

SI model parameters from ROB
SI model parameters from GRI
Mass Fraction Remaining
1.0
0.8
0.6
0.4
0.2
0.0
a
b
Total model SOA:
Start of aging simulation
Day 1
Day 2
Day 3
MILAGRO observed:
Total OOA
SV-OOA
LV-OOA
50
100
150
200
TD Temperature (°C)

Figure S9

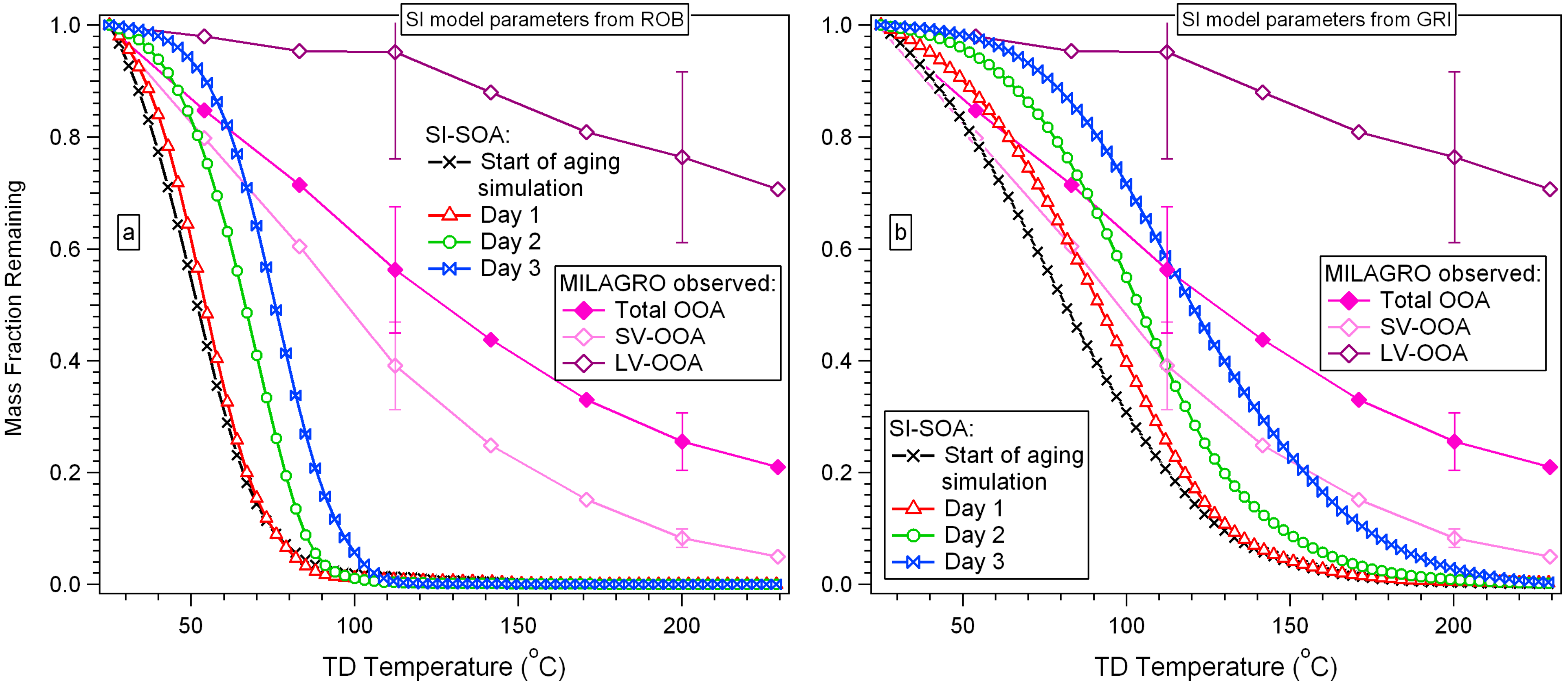

SI model parameters from ROB
SI-SOA:
Start of aging simulation
Day 1
Day 2
Day 3
MILAGRO observed:
Total OOA
SV-OOA
LV-OOA
a
Mass Fraction Remaining
TD Temperature (°C)
SI model parameters from GRI
MILAGRO observed:
Total OOA
SV-OOA
LV-OOA
SI-SOA:
Start of aging simulation
Day 1
Day 2
Day 3
b
TD Temperature (°C)

Figure S10

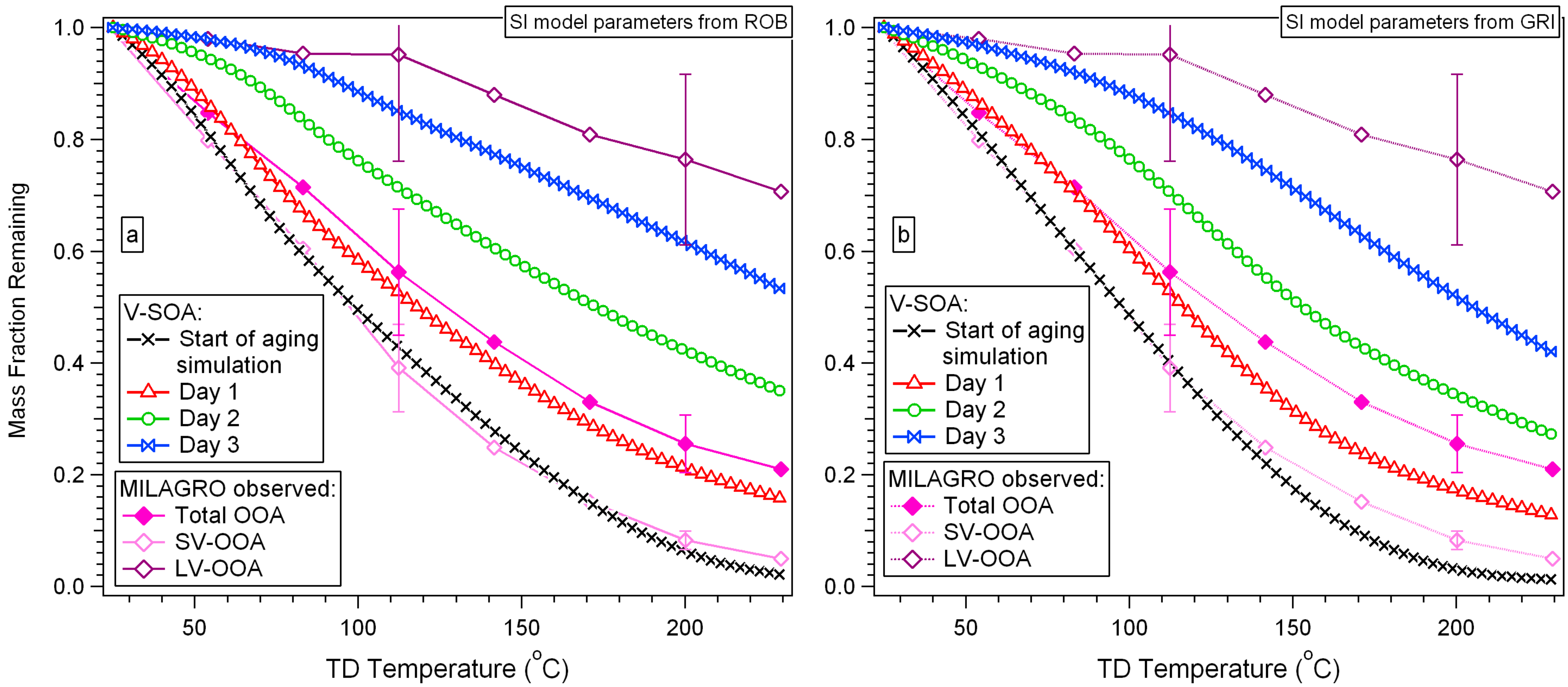

SI model parameters from ROB
SI model parameters from GRI
a
b
Mass Fraction Remaining
TD Temperature (°C)
V-SOA:
Start of aging simulation
Day 1
Day 2
Day 3
MILAGRO observed:
Total OOA
SV-OOA
LV-OOA
1.0
0.8
0.6
0.4
0.2
0.0
50
100
150
200

Figure S11

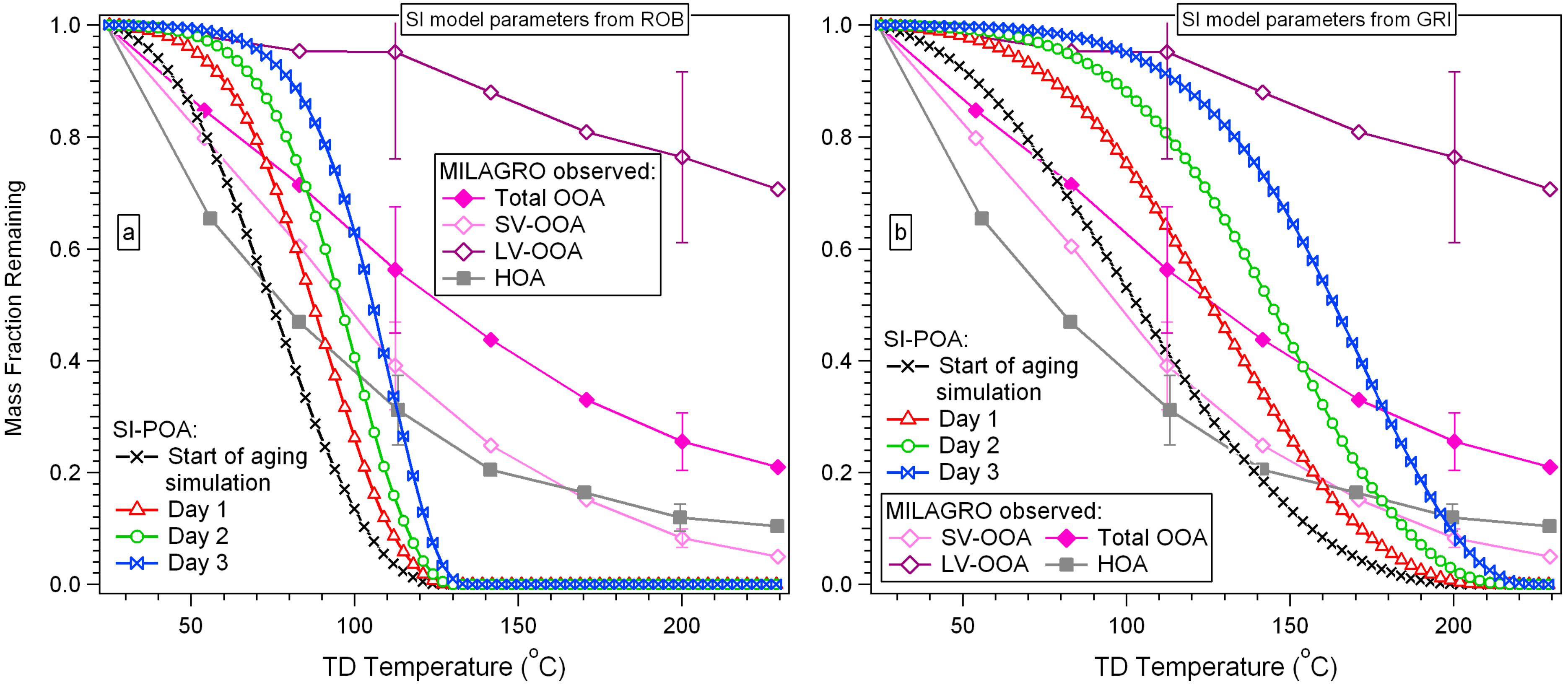

SI model parameters from ROB
Mass Fraction Remaining
a
MILAGRO observed:
Total OOA
SV-OOA
LV-OOA
HOA
SI-POA:
Start of aging simulation
Day 1
Day 2
Day 3
TD Temperature (°C)
SI model parameters from GRI
b
SI-POA:
Start of aging simulation
Day 1
Day 2
Day 3
MILAGRO observed:
SV-OOA
Total OOA
LV-OOA
HOA
TD Temperature (°C)

Figure S12

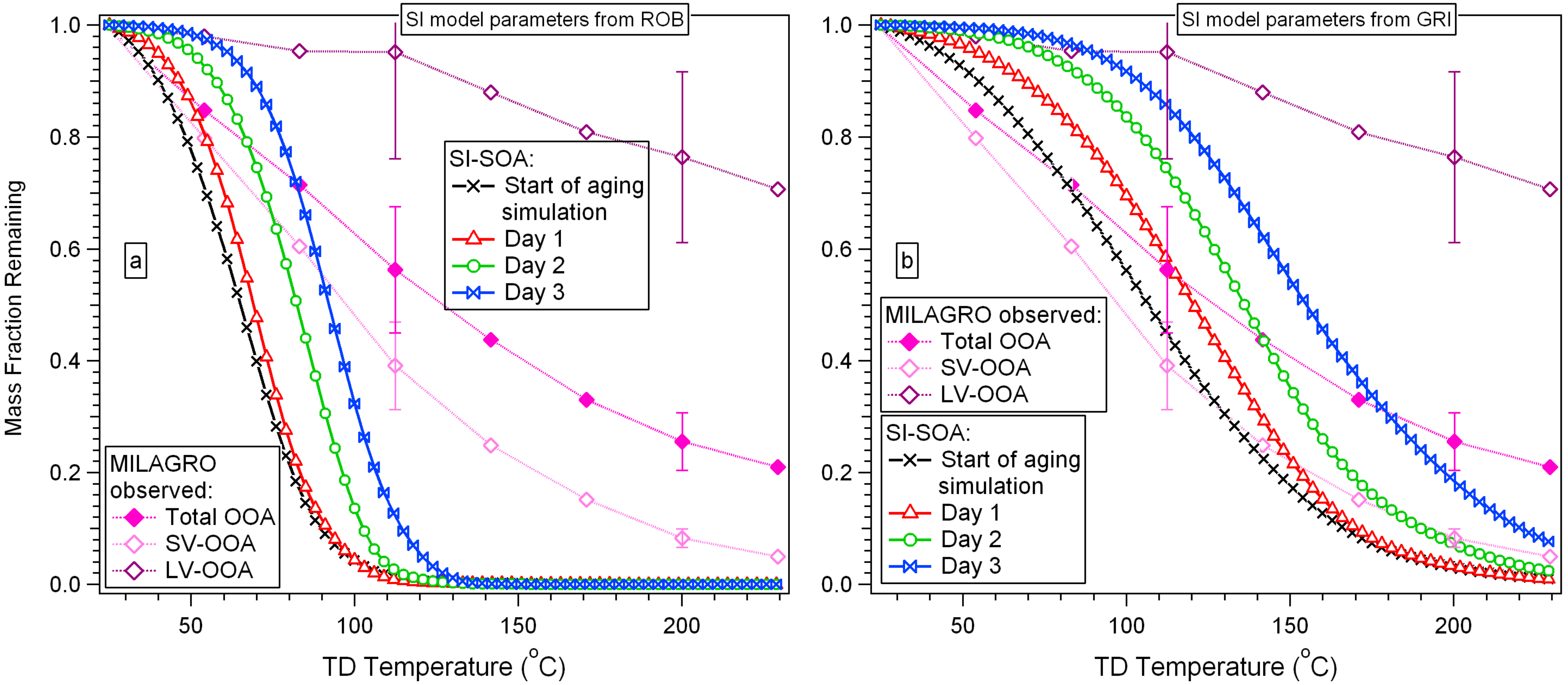

SI model parameters from ROB
SI model parameters from GRI
a
b
Mass Fraction Remaining
TD Temperature (°C)
SI-SOA:
Start of aging simulation
Day 1
Day 2
Day 3
MILAGRO observed:
Total OOA
SV-OOA
LV-OOA

Figure S13

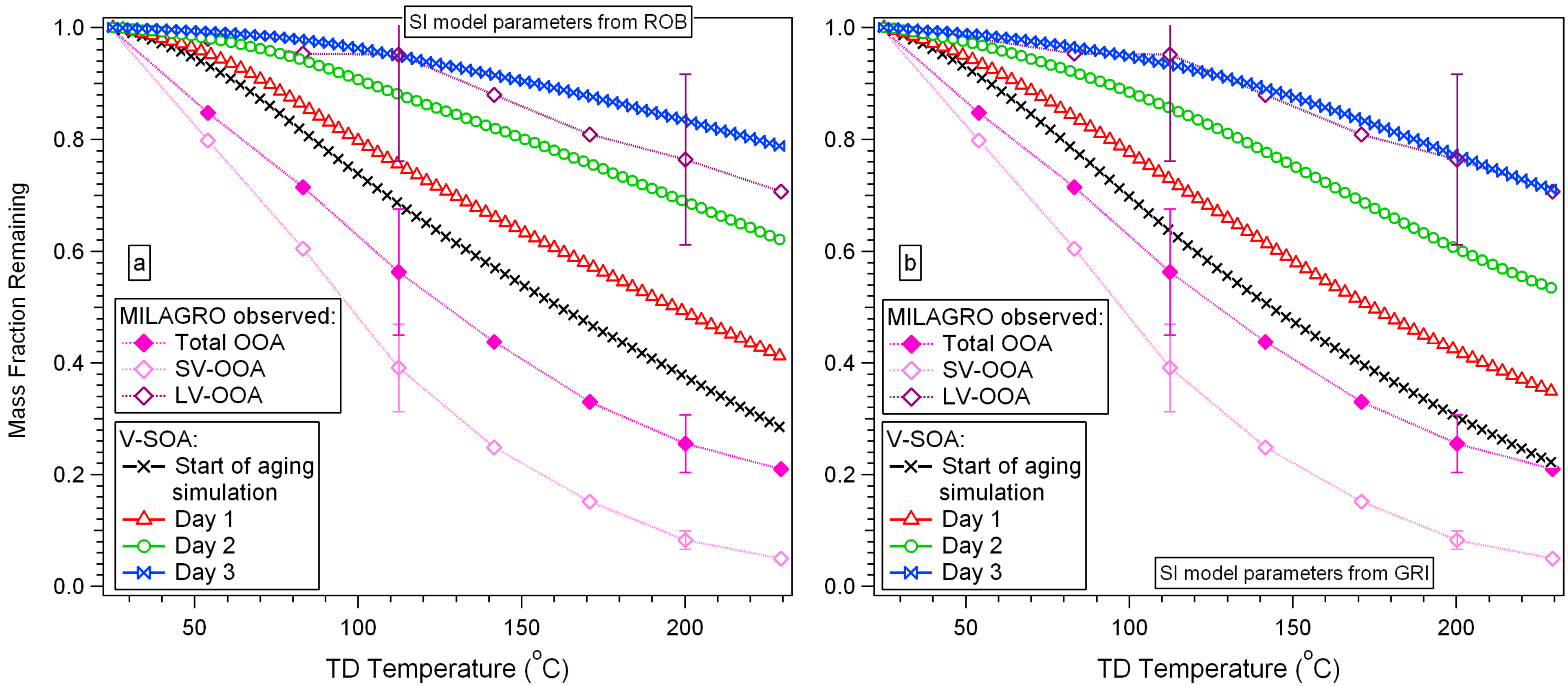

SI model parameters from ROB
a
b
Mass Fraction Remaining
MILAGRO observed:
Total OOA
SV-OOA
LV-OOA
V-SOA:
Start of aging simulation
Day 1
Day 2
Day 3
TD Temperature (°C)
SI model parameters from GRI

Figure S14

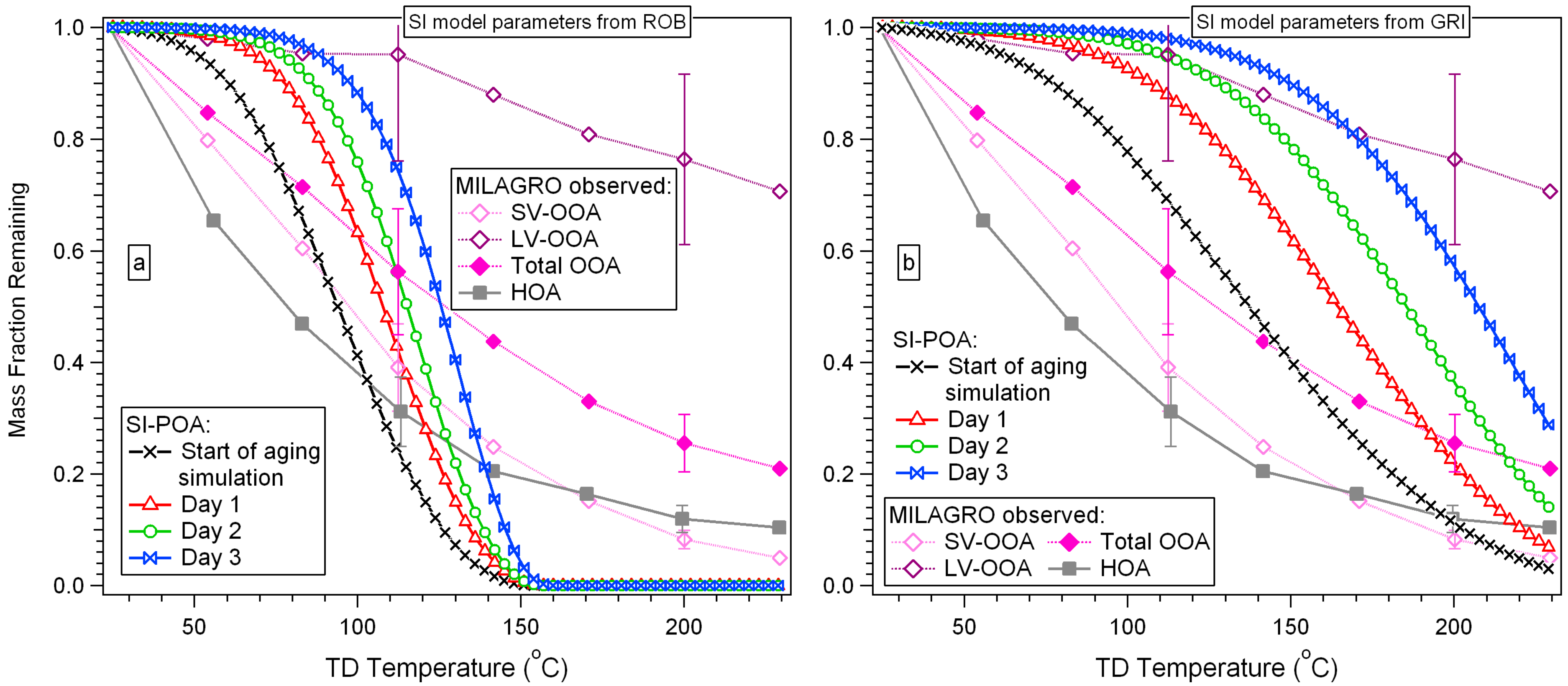

SI model parameters from ROB
SI model parameters from GRI
Mass Fraction Remaining
TD Temperature (°C)
a
b
MILAGRO observed:
SV-OOA
LV-OOA
Total OOA
HOA
SI-POA:
Start of aging simulation
Day 1
Day 2
Day 3

Figure S15

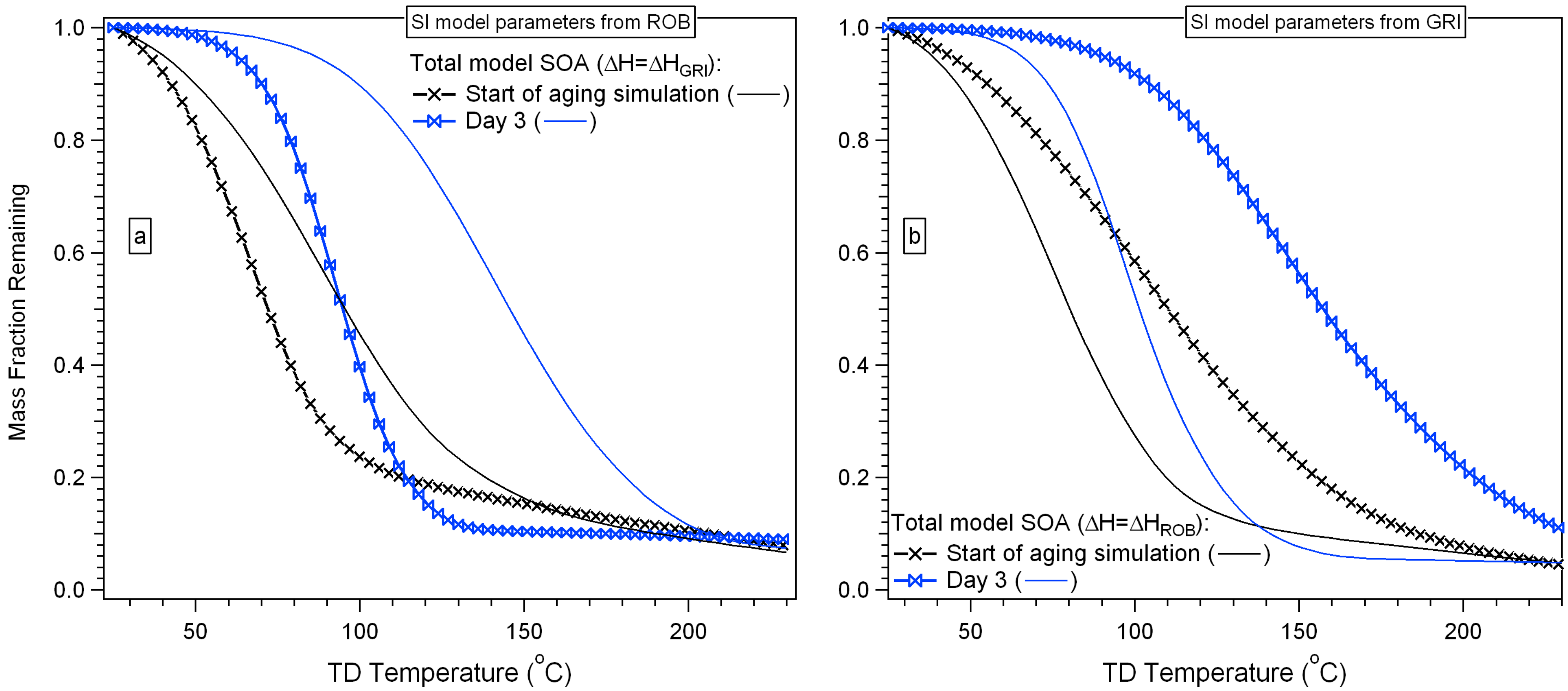
SI model parameters from ROB
Total model SOA (ΔH=ΔH_GRI):
Start of aging simulation (——)
Day 3 (——)
a
Mass Fraction Remaining
1.0
0.8
0.6
0.4
0.2
0.0
50
100
150
200
TD Temperature (°C)
SI model parameters from GRI
Total model SOA (ΔH=ΔH_ROB):
Start of aging simulation (——)
Day 3 (——)
b
1.0
0.8
0.6
0.4
0.2
0.0
50
100
150
200
TD Temperature (°C)

Figure S16

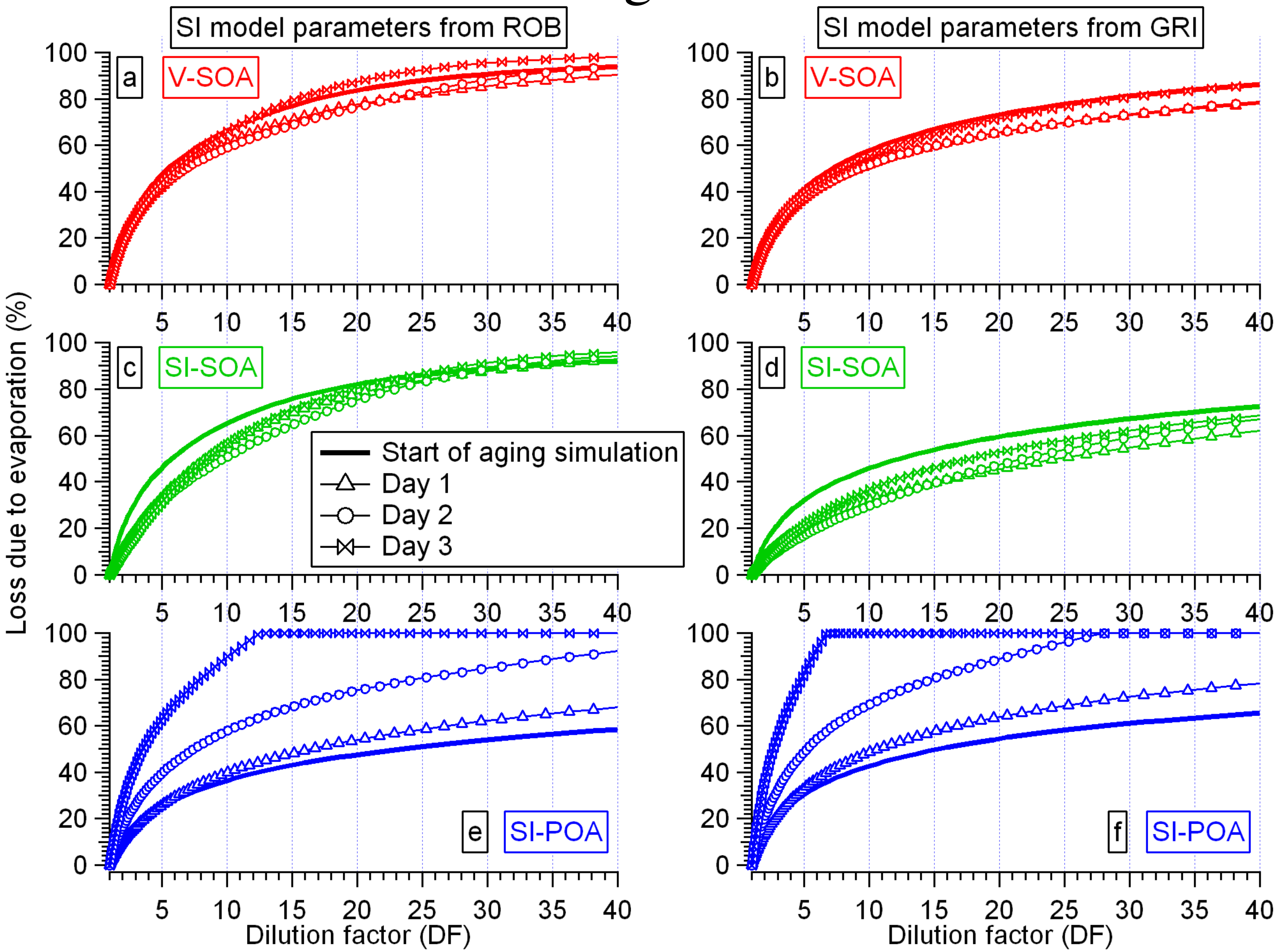

SI model parameters from ROB
SI model parameters from GRI
a
V-SOA
b
V-SOA
c
SI-SOA
d
SI-SOA
e
SI-POA
f
SI-POA
Start of aging simulation
Day 1
Day 2
Day 3
Loss due to evaporation (%)
Dilution factor (DF)
Dilution factor (DF)
0
20
40
60
80
100
5
10
15
20
25
30
35
40

Figure S17

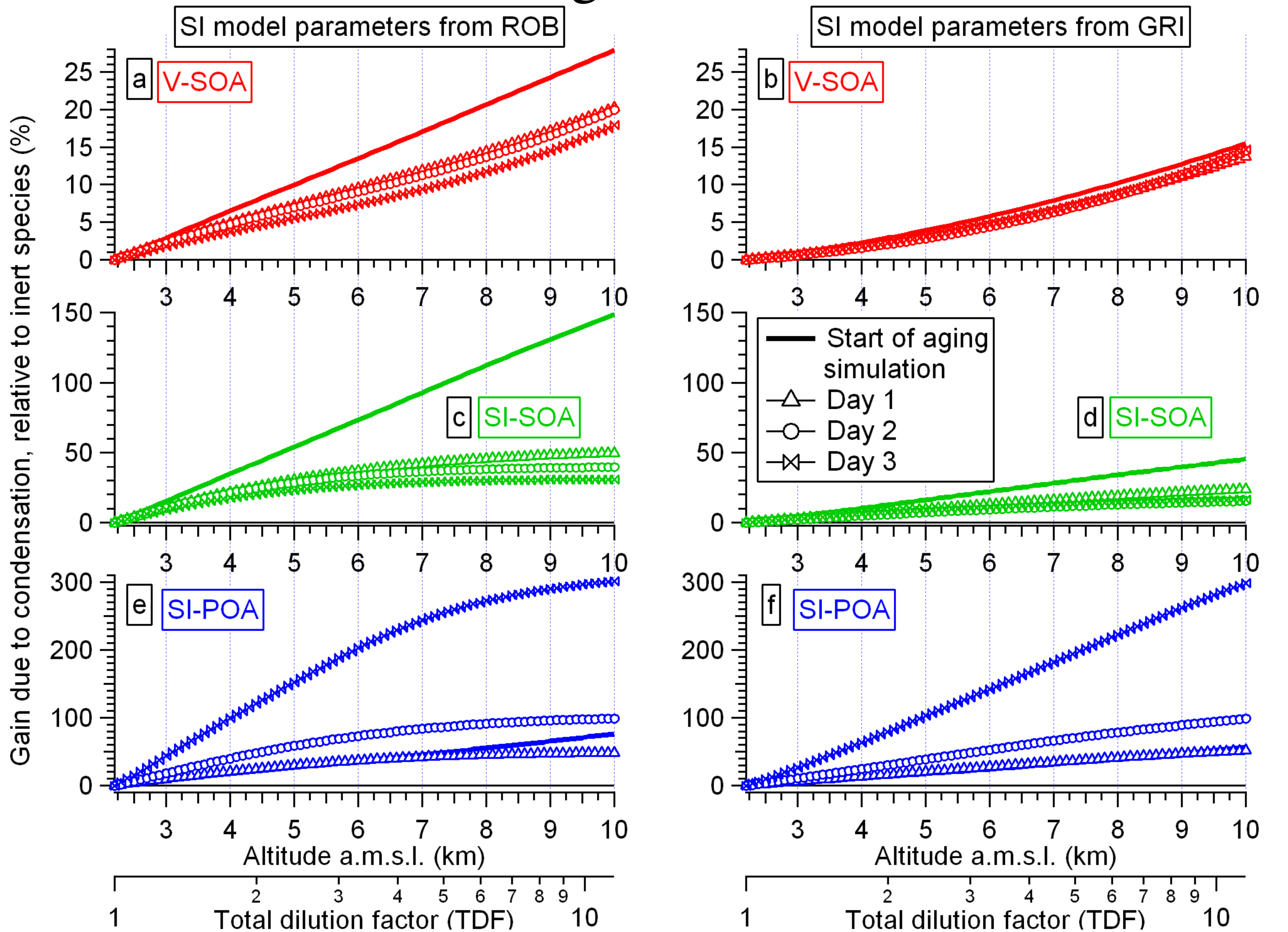

SI model parameters from ROB
SI model parameters from GRI
a
V-SOA
b
V-SOA
c
SI-SOA
d
SI-SOA
e
SI-POA
f
SI-POA
Start of aging simulation
Day 1
Day 2
Day 3
Gain due to condensation, relative to inert species (%)
Altitude a.m.s.l. (km)
Total dilution factor (TDF)

Figure S18

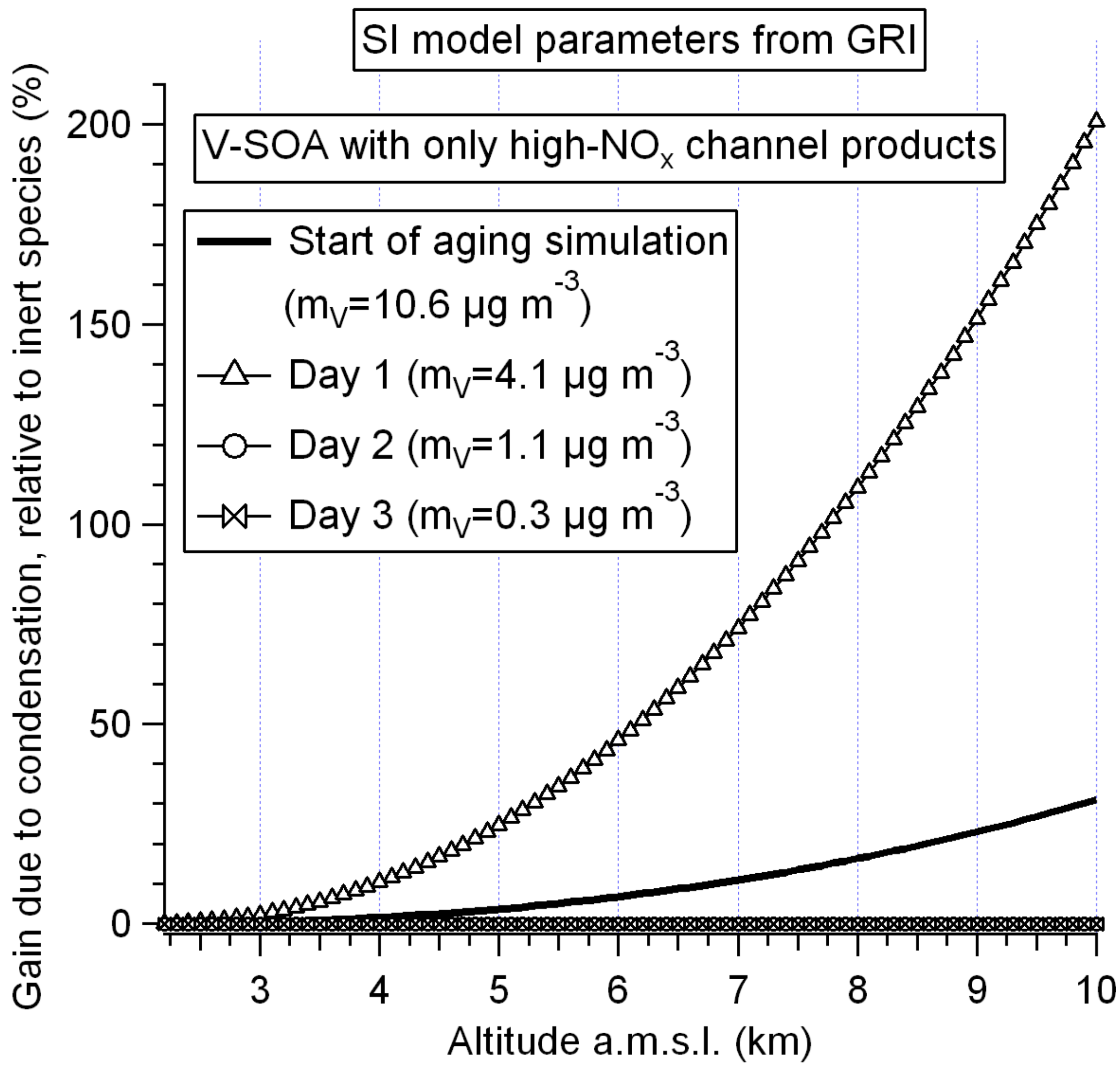

SI model parameters from GRI
V-SOA with only high-NOx channel products
Start of aging simulation
(mV=10.6 µg m-3)
Day 1 (mV=4.1 µg m-3)
Day 2 (mV=1.1 µg m-3)
Day 3 (mV=0.3 µg m-3)
Gain due to condensation, relative to inert species (%)
0
50
100
150
200
3
4
5
6
7
8
9
10
Altitude a.m.s.l. (km)